Published June 17, 2013

The tumor suppressor CDKN3 controls mitosis

Grzegorz Nalepa, Jill Barnholtz-Sloan, Rikki Enzor, Dilip Dey, Ying He, Jeff R. Gehlhausen, Amalia S. Lehmann, Su-Jung Park, Yanzhu Yang, Xianlin Yang, Shi Chen, Xiaowei Guan, Yanwen Chen, Jamie Renbarger, Feng-Chun Yang, Luis F. Parada, and Wade Clapp

Vol. 201 No. 7, June 24, 2013. Pages 997–1012.

The authors noticed an unintended Western blot panel in the original version of Fig. 1. The authors have indicated that this was due to a clerical error during figure revision. A corrected version of Fig. 1 is shown below.

The html and pdf versions of this article have been corrected. The error remains only in the print version.

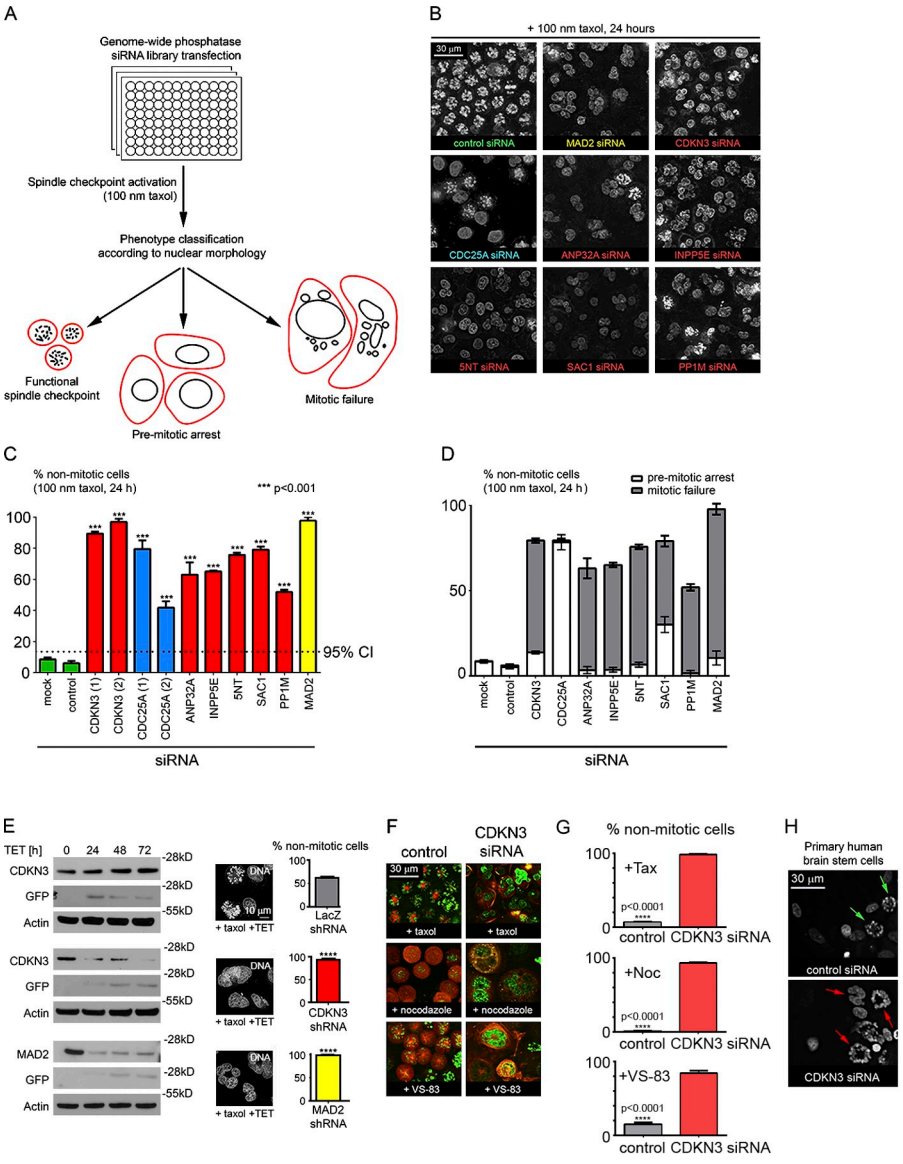

Figure 1. **Functional siRNA screen reveals candidate mitotic phosphatases.** (A) Screen schematic. 801 siRNAs targeting 267 phosphatases were used in the screen. (B) Nuclear morphology of cells transfected with indicated siRNAs and treated with 100 nm taxol for 24 h 2 d after siRNA transfection. Negative control cells arrest in mitosis when exposed to taxol. Multinucleation resulting from SAC failure occurs in cells transfected with siRNAs targeting CDKN3, ANP32A, INPP5E, 5NT, SAC1, and PP1M as well as MAD2 (positive control). CDC25A knockdown results in premitotic arrest. (C) Quantification of screen results. Broken lines: 95% confidence interval. P-values were calculated using one-way ANOVA. n = 3 counts for each siRNA (a single representative experiment out of two repeats). Error bars represent mean values ± SEM. (D) Subquantification of phenotypes into premitotic arrest versus multinucleation. Knockout of all screen hits except for CDC25A results in SAC failure. Error bars represent mean values of three independent counts (n = 3). (E) Generation of cell lines expressing tetracycline-inducible shRNAs and GFP. Western blots show target knockdown as a function of time in response to shRNA induction. The SAC failure in MAD2 and CDKN3 shRNA cells is indicated by a decreased phospho-H3 fraction in cells exposed to 100 nm taxol for 24 h after 72 h of tetracycline induction ($P < 0.0001$ for MAD2 and CDKN3 shRNA cells compared with LACZ shRNA cells in one-way ANOVA; n = 10). Error bars show mean values ± SEM. (F) CDKN3 knockout cells fail to activate the spindle checkpoint in response to three mitotic poisons. (G) CDKN3 knockdown disrupts the SAC response to three spindle poisons. HeLa$^{GFP\text{-}H2B/mCherry\text{-}\alpha\text{-}tubulin}$ cells were transfected with control and CDKN3 siRNAs, and 48 h later treated with inhibitors for 24 h. Cells were fixed and imaged to count nuclear fractions. n = 3 counts per siRNA per condition. $P < 0.0001$ (t test). Error bars represent mean values ± SEM. (H) CDKN3 is essential for the spindle checkpoint in human primary brain stem cells. The SC-23 cells were challenged with 200 nm taxol 72 h after siRNA transfection. Mitotic arrest occurs in control cells (green arrows), and CDKN3 knockdown led to multinucleation (red arrows).

Supplemental Material can be found at:
/content/suppl/2013/06/13/jcb.201205125.DC1.html

The tumor suppressor CDKN3 controls mitosis

Grzegorz Nalepa,[1,4] Jill Barnholtz-Sloan,[5] Rikki Enzor,[1] Dilip Dey,[1] Ying He,[1] Jeff R. Gehlhausen,[1] Amalia S. Lehmann,[1] Su-Jung Park,[1] Yanzhu Yang,[1] Xianlin Yang,[1] Shi Chen,[1] Xiaowei Guan,[5] Yanwen Chen,[5] Jamie Renbarger,[1,4] Feng-Chun Yang,[1] Luis F. Parada,[6] and Wade Clapp[1,2,3]

[1]Department of Pediatrics, Herman B Wells Center for Pediatric Research, [2]Department of Microbiology and Immunology, [3]Department of Biochemistry and Molecular Biology, and [4]Division of Pediatric Hematology-Oncology, Riley Hospital for Children, Indiana University School of Medicine, Indianapolis, IN 46202
[5]Case Western Reserve University Comprehensive Cancer Center, Cleveland, OH 44106
[6]Department of Developmental Biology, University of Texas Southwestern Medical Center, Dallas, Texas 75390

Mitosis is controlled by a network of kinases and phosphatases. We screened a library of small interfering RNAs against a genome-wide set of phosphatases to comprehensively evaluate the role of human phosphatases in mitosis. We found four candidate spindle checkpoint phosphatases, including the tumor suppressor CDKN3. We show that CDKN3 is essential for normal mitosis and G1/S transition. We demonstrate that subcellular localization of CDKN3 changes throughout the cell cycle. We show that CDKN3 dephosphorylates threonine-161 of CDC2 during mitotic exit and we visualize CDC2$^{pThr\text{-}161}$ at kinetochores and centrosomes in early mitosis. We performed a phosphokinome-wide mass spectrometry screen to find effectors of the CDKN3-CDC2 signaling axis. We found that one of the identified downstream phosphotargets, CKβ phosphorylated at serine 209, localizes to mitotic centrosomes and controls the spindle checkpoint. Finally, we show that CDKN3 protein is down-regulated in brain tumors. Our findings indicate that CDKN3 controls mitosis through the CDC2 signaling axis. These results have implications for targeted anticancer therapeutics.

Introduction

Abnormal mitosis jeopardizes genome integrity (Ganem et al., 2009) and causes aneuploidy, which is both a cause and a consequence of cancer (Gordon et al., 2012). Multiple checkpoints ensure the high fidelity of mitosis (Musacchio and Salmon, 2007; Thompson et al., 2010; Hanahan and Weinberg, 2011). The spindle assembly checkpoint (SAC; for review see Musacchio and Salmon, 2007) is a signaling cascade that prevents premature separation of sister chromatids by delaying the metaphase-to-anaphase transition until all the kinetochores are properly attached to the spindle (Hoyt et al., 1991; Li and Murray, 1991). Then, a cascade of signals triggers chromosome segregation, leading to mitotic exit. The canonical mitotic exit pathway is initiated by the release of the APC/C^{CDC20} ubiquitin ligase from the SAC-mediated inhibition (Sudakin et al., 2001), which leads to the proteasomal degradation of cyclin B and a drop in mitotic cyclin-dependent kinase (CDC2/CDK1–cyclin B) activity. Work performed in *Xenopus laevis* egg extracts suggests that the residual CDK activity may be silenced through dephosphorylation of activating threonine-161 of CDC2 (Lorca et al., 1992) to ensure normal exit from mitosis. However, the role of CDC2^{pThr161} dephosphorylation in mammalian cells remains to be shown.

System-biology studies are dissecting the connections between the SAC and the CDK activity oscillations (Bouchoux and Uhlmann, 2011). High CDC2 activity maintains the SAC (D'Angiolella et al., 2003). After the SAC is satisfied, degradation of cyclin B is followed by sequential inactivation of CDK targets (Bouchoux and Uhlmann, 2011). The irreversible mitotic exit depends on this anti-CDK feedback loop (López-Aviles et al., 2009), and multiple phosphatase pathways converge here to ensure safe passage through mitosis (for a recent review see Wurzenberger and Gerlich, 2011). For example, the decreased activity of the CDK-Greatwall-ENSA/ARPP19 signaling axis upon the SAC release activates the PP2A phosphatase (Burgess et al., 2010; Gharbi-Ayachi et al., 2010; Mochida et al., 2010) to control the mitotic exit (Burgess et al., 2010), presumably through dephosphorylation of key CDK targets (Schmitz et al., 2010). Given the complexity of these signaling networks, additional mitotic exit phosphatases will likely be discovered.

Correspondence to Wade Clapp: dclapp@iupui.edu

Abbreviations used in this paper: ANOVA, analysis of variance; EdU, 5-ethynyl-2′-deoxyuridine; GBM, glioblastoma multiforme; NEB, nuclear envelope breakdown; SAC, spindle assembly checkpoint.

The Rockefeller University Press $30.00
J. Cell Biol. Vol. 201 No. 7 997–1012
www.jcb.org/cgi/doi/10.1083/jcb.201205125

The mitotic signaling networks have clinical importance. Although weakened SAC promotes aneuploidy and cancer (Cahill et al., 1998; Dai et al., 2004; Hanks et al., 2004), complete loss of control over the mitotic exit is lethal for mammalian cells (Michel et al., 2001), including cancer cells (Kops et al., 2004). Genetic disruption of the PP2A–CDK signaling causes tumor regression in a mouse cancer model (Manchado et al., 2010), and targeting late mitosis with small molecules induces cancer death in vivo (Tao et al., 2005). Thus, the mitotic exit is a target for anticancer chemotherapies (Nalepa et al., 2006; Gordon et al., 2012). Therapies against aneuploid cells may be useful in cancers that use chromosomal instability to resist treatment. Glioblastoma multiforme (GBM), the most common primary malignant brain cancer, exemplifies this type of genomically unstable tumor (Cancer Genome Atlas Research Network, 2008; Parsons et al., 2008; Mir et al., 2010; Ohba et al., 2011). Despite the most aggressive therapies, glioblastoma is uniformly lethal (Stupp et al., 2005). Therefore, identification of drug targets in GBM is clinically important.

In this work, we describe a systematic RNAi screen against a genome-wide set of phosphatases that revealed candidate regulators of the SAC. We show that one of these phosphatases, CDKN3, associates with centrosomes and dephosphorylates $CDC2^{pThr\text{-}161}$, presumably contributing to the CDK inactivation at the mitotic exit. We visualize $CDC2^{pThr\text{-}161}$ at kinetochores and centrosomes in early mitosis, which suggests a spatiotemporal connection between CDKN3 and the SAC. We demonstrate that CDKN3 regulates the G1/S transition, and we describe how the CDKN3 localization changes throughout the cell cycle. We show that loss of CDKN3 leads to abnormal mitosis and generation of supernumerary centrosomes. We discuss the results of our phosphoproteomic screen, which revealed multiple late-mitotic effectors of CDKN3. We show that one of these phosphotargets ($CK\beta^{pS209}$) is essential for the SAC and localizes to centrosomes. Finally, we revisit the previously postulated connection between CDKN3 and carcinogenesis. Because previous studies regarding CDKN3 expression in GBMs generated ambiguous results (Yeh et al., 2000; Blenk et al., 2007; Padua and Hansen, 2009; Taylor et al., 2010), we analyzed CDKN3 protein expression in two independent patient-derived GBM cohorts. We found decreased CDKN3 protein in a fraction of GBMs, accompanied by increased CDK activity. Together, these findings offer new insights into the regulation of human cell division and provide a conceptual framework for rationally designed therapies in GBM and other cancers.

Results

A functional genomic screen identifies the role of CDKN3 in mitosis

To identify human SAC phosphatases, we screened an siRNA library against a genome-wide set of human phosphatases. HeLa cells were transfected with library siRNAs on 96-well plates and challenged with taxol. Cells were then fixed and imaged under a high-throughput microscope (Fig. 1 A). Cells transfected with an siRNA targeting MAD2 (a known SAC regulator; Dobles et al., 2000) became multinucleated due to SAC failure, whereas negative control cells arrested in prometaphase (Fig. 1 B). Of 801 siRNAs, seven (0.87%) produced the multinucleated phenotype upon taxol treatment, which is consistent with SAC failure (Fig. 1, B–D). Additionally, two siRNAs targeting CDC25A induced premitotic arrest in accordance with the known function of the CDC25 phosphatases in mitotic entry (for review see De Wulf et al., 2009). The candidate SAC genes found in our screen included SAC-1 (a phosphatase that regulates mitotic spindle stability; Liu et al., 2008); ANP32A (a regulator of the PP2A phosphatase; Habrukowich et al., 2010); and three phosphatases that had not been linked to mitosis: INPP5E, 5NT, and PP1M. Finally, the siRNAs that generated the strongest SAC failure phenotype targeted the double-specificity phosphatase, CDKN3. CDKN3 dephosphorylates interphase CDKs (Gyuris et al., 1993; Hannon et al., 1994), but its role in mitosis has not been reported.

We generated stable T-REx HeLa cells expressing Tet-inducible CDKN3 shRNA as another validation tool (Table S2). The inducible knockdown of CDKN3 resulted in SAC failure similar to the MAD2 knockdown (Fig. 1 E). We found that CDKN3 is required for mitotic arrest in response to other spindle poisons (nocodazole and VS-83) that are mechanistically different from taxol (Sawin et al., 1992; Mayer et al., 1999; Fig. 1, F and G). Finally, we found that CDKN3 is essential for the spindle checkpoint in neural progenitor cells isolated from postmortem human cortex (Schwartz et al., 2003; Fig. 1 H). This last observation suggests that the CDKN3-dependent SAC may operate in the human brain, which is consistent with the proposed tumor suppressor role for CDKN3 in brain tumors (Yu et al., 2007).

The SAC regulator MAD2 is sensitive to off-target knockdown (Sigoillot et al., 2012), which may hamper validation of siRNAs (Hübner et al., 2010; Westhorpe et al., 2010). Thus, we comprehensively validated our findings to exclude the possibility of an off-target effect. First, we showed that the CDKN3 siRNA SAC phenotype is partially rescued by overexpression of siRNA-resistant GFP-CDKN3 (Fig. 2, A and B). Second, we recapitulated the SAC phenotype resulting from CDKN3 knockdown with three other CDKN3 siRNAs not included in the library (Fig. 2, C and D). Third, we found normal MAD2 protein levels in cells transfected with the CDKN3 siRNAs using quantitative infrared Western blots (Fig. 2, E–G). Fourth, we confirmed normal MAD2 localization in prometaphase cells transfected with the CDKN3 siRNAs (Fig. 2, G and H). Finally, ectopic expression of MAD2 did not rescue the SAC in cells transfected with CDKN3 siRNA (Fig. 2, I–K). We noted that overexpression of MAD2 disrupts the SAC (Fig. 2 I), which is consistent with the proposed contribution of increased MAD2 to chromosome instability (Sotillo et al., 2007, 2010). Together, these experiments indicate that the SAC deficiency observed in CDKN3 knockdown cells is not caused by an off-target effect.

CDKN3 has been linked to cancer (Yeh et al., 2000; Niculescu et al., 2004; Blenk et al., 2007; Yu et al., 2007; Padua and Hansen, 2009; Jiang et al., 2010; Taylor et al., 2010), but the mechanistic connection between CDKN3 and carcinogenesis was lacking. Thus, we decided to further dissect cell cycle pathways controlled by CDKN3 with particular attention to mitosis.

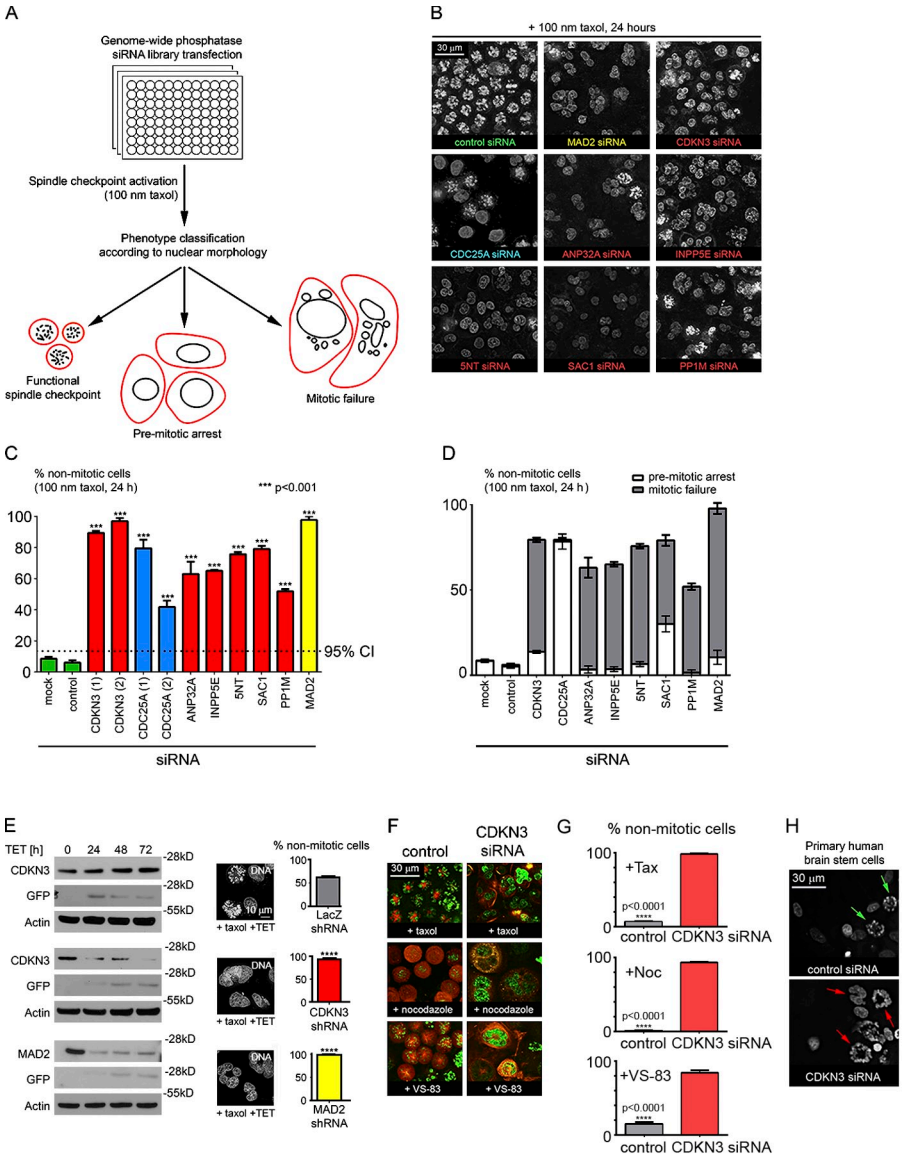

Figure 1. **Functional siRNA screen reveals candidate mitotic phosphatases.** (A) Screen schematic. 801 siRNAs targeting 267 phosphatases were used in the screen. (B) Nuclear morphology of cells transfected with indicated siRNAs and treated with 100 nm taxol for 24 h 2 d after siRNA transfection. Negative control cells arrest in mitosis when exposed to taxol. Multinucleation resulting from SAC failure occurs in cells transfected with siRNAs targeting CDKN3, ANP32A, INPP5E, 5NT, SAC1, and PP1M as well as MAD2 (positive control). CDC25A knockdown results in premitotic arrest. (C) Quantification of screen results. Broken lines: 95% confidence interval. P-values were calculated using one-way ANOVA. $n = 3$ counts for each siRNA (a single representative experiment out of two repeats). Error bars represent mean values ± SEM. (D) Subquantification of phenotypes into premitotic arrest versus multinucleation. Knockout of all screen hits except for CDC25A results in SAC failure. Error bars represent mean values of three independent counts ($n = 3$). (E) Generation of cell lines expressing tetracycline-inducible shRNAs and GFP. Western blots show target knockdown as a function of time in response to shRNA induction. The SAC failure in MAD2 and CDKN3 shRNA cells is indicated by a decreased phospho-H3 fraction in cells exposed to 100 nm taxol for 24 h after 72 h of tetracycline induction ($P < 0.0001$ for MAD2 and CDKN3 shRNA cells compared with LACZ shRNA cells in one-way ANOVA; $n = 10$). Error bars show mean values ± SEM. (F) CDKN3 knockout cells fail to activate the spindle checkpoint in response to three mitotic poisons. (G) CDKN3 knockdown disrupts the SAC response to three spindle poisons. HeLa$^{GFP\text{-}H2B/mCherry\text{-}\alpha\text{-}tubulin}$ cells were transfected with control and CDKN3 siRNAs, and 48 h later treated with inhibitors for 24 h. Cells were fixed and imaged to count nuclear fractions. $n = 3$ counts per siRNA per condition. $P < 0.0001$ (*t* test). Error bars represent mean values ± SEM. (H) CDKN3 is essential for the spindle checkpoint in human primary brain stem cells. The SC-23 cells were challenged with 200 nm taxol 72 h after siRNA transfection. Mitotic arrest occurs in control cells (green arrows), and CDKN3 knockdown led to multinucleation (red arrows).

CDKN3 is required for normal mitosis

We assessed the morphology of CDKN3 knockdown cells grown in the absence of taxol. We observed multinucleation in CDKN3 and MAD2 knockdown cells (Fig. 3, A and B). Because multinucleation is a symptom of chromosome missegregation or cytokinesis failure, this suggests a role for CDKN3 in unperturbed mitosis. We noted decreased mitotic fraction in unsynchronized CDKN3- and MAD2-deficient cells (Fig. 3 C), which suggests that loss of CDKN3 may accelerate mitosis similarly to MAD2 down-regulation (Meraldi et al., 2004).

To test whether CDKN3 knockdown accelerates mitosis, we used time-lapse imaging (Fig. 3, C–E). We found that CDKN3-deficient cells complete mitosis faster than control cells (Fig. 3, D–E), with increased frequency of abnormal mitoses (Fig. 3, F and G). Representative time-lapse videos are shown on Videos 1–6. Thus, CDKN3 is essential not only for cellular response to spindle poisons, but also for the unperturbed cell division.

CDKN3 localizes to nucleoli in interphase and controls progression through interphase

We found that endogenous CDKN3 is a nuclear protein in interphase (Fig. 4 A). Extraction of soluble proteins revealed endogenous CDKN3 targeted to intranucleolar foci (Fig. 4 A) within nucleolin clusters (Fig. 4 B and Fig. S1). Overexpressed GFP-CDKN3 showed similar localization (Fig. 4 C and Fig. S1). The nuclear targeting of CDKN3 is independent of the CDKN3 phosphatase activity, as the phosphatase-dead CDKN3 mutant exhibits normal localization (Fig. 4 C).

CDKN3 is an interphase CDK inhibitor (Gyuris et al., 1993; Hannon et al., 1994). Therefore, we wondered whether CDKN3 knockdown will facilitate the G1/S transition. Indeed, we observed a slightly increased S-phase fraction of unsynchronized CDKN3 knockdown cells at the cost of the G1-phase fraction (Fig. 4, D and E). More dramatically, loss of CDKN3 attenuated starvation-induced G1 arrest (Fig. 4 F).

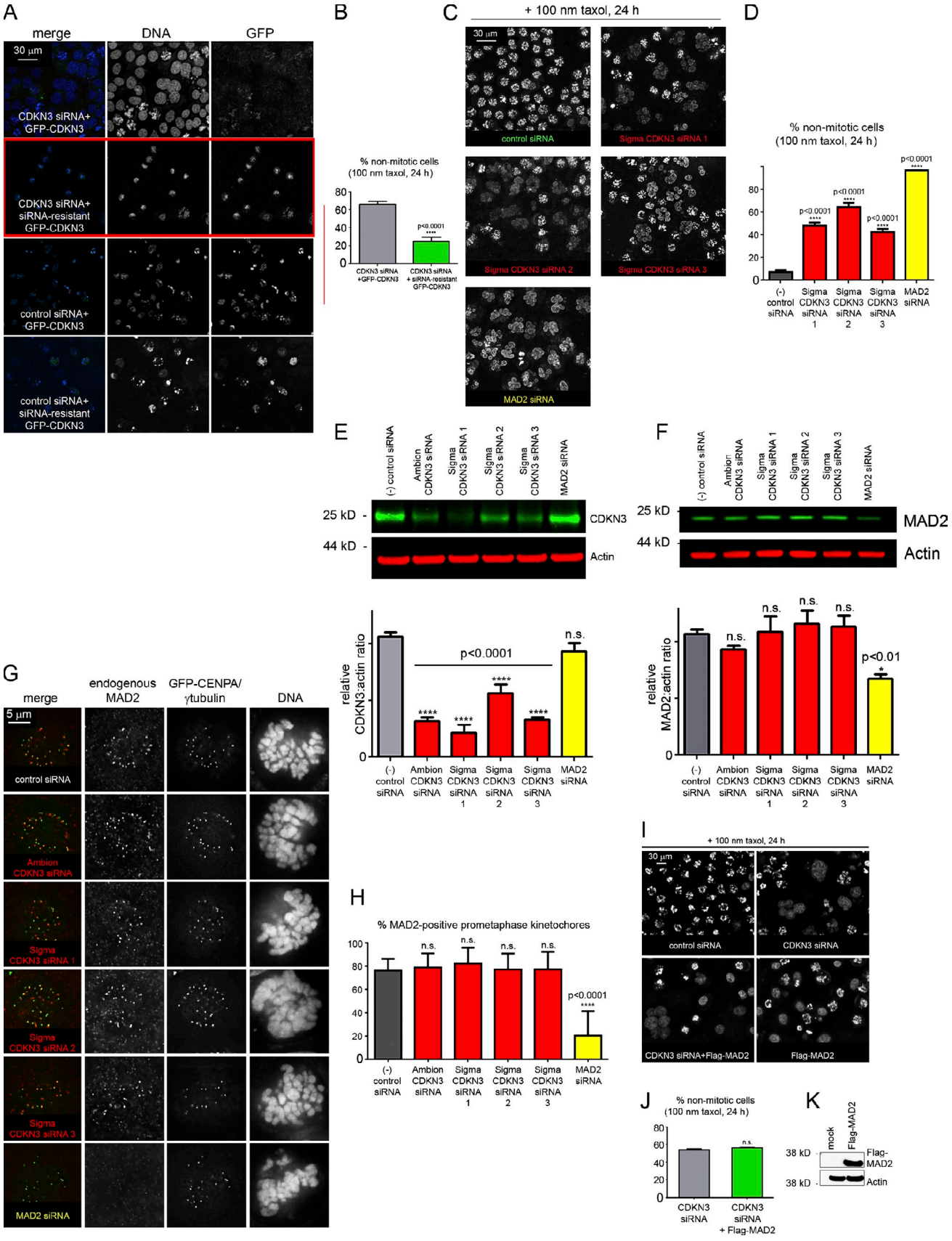

Figure 2. **Spindle checkpoint failure in CDKN3 siRNA-treated cells is not caused by off-target RNAi effects.** (A) Overexpression of siRNA-resistant GFP-CDKN3 rescues the SAC failure phenotype in cells transfected with CDKN3 siRNA. Phenotype rescue in CDKN3 knockdown cells transfected with siRNA-resistant GFP-CDKN3 is indicated by mitotic arrest in taxol (red). No phenotype rescue and minimal GFP fluorescence were observed in CDKN3

CDKN3 localizes to centrosomes

We next tracked CDKN3 localization during mitosis. We found that endogenous CDKN3 associates with centrosomes (Fig. 5 A). We confirmed this finding using a HeLa cell line stably expressing DDK-tagged CDKN3 (Fig. 5 B). Some endogenous CDKN3 is seen at the midzone spindle in anaphase (Fig. 5 C). In telophase, the majority of CDKN3 returns to the newly formed nuclei (Fig. 5, A and B). A small fraction of CDKN3 may associate with the midbody, as suggested by detection of a weak immunofluorescence signal in stable DDK-CDKN3–overexpressing cells next to the KIF20A-labeled midbody (Hümmer and Mayer, 2009; Lee et al., 2010) in late mitosis (Fig. 5 D). Some CDKN3 remains at the centrosomes in interphase (Fig. 5, E and F; and Fig. S2). The association of CDKN3 with the mitotic apparatus during cell division is consistent with the role for CDKN3 in mitosis.

We noted increased centrosome numbers in CDKN3 knockdown cells (Fig. 6, A and B). Although it remains to be determined whether accumulation of centrosomes in CDKN3-knockdown cells is a consequence of failed cytokinesis or abnormal centrosome replication, this finding implies that the centrosome-associated phosphatase CDKN3 is critical for the maintenance of normal centrosome numbers.

CDKN3 controls final stages of mitosis by dephosphorylating CDC2 at Thr-161

The structure of the phospho-CDK2–CDKN3 complex has been solved (Poon and Hunter, 1995; Song et al., 2001). The examination of a spatial overlay of CDK2 and the mitotic cyclin-dependent kinase CDC2 reveals perfect conservation of the CDKN3 docking interface (Fig. 7 A). CDKN3 physically binds CDC2 (Gyuris et al., 1993; Hannon et al., 1994). Thus, we examined whether CDKN3 dephosphorylates CDC2 at Thr-161.

We visualized CDC2 phosphorylated at Thr-161 in dividing cells. During mitosis, CDC2 localizes to centrosomes, as described previously (De Souza et al., 2000), and colocalizes with CDKN3 (Fig. 7 B). Upon mitotic entry, CDC2 is phosphorylated at Thr-161 (Fig. 7 C). After nuclear envelope breakdown (NEB), $CDC2^{pThr\text{-}161}$ is found at centrosomes, kinetochores, and the spindle (Fig. 7, C and D). In anaphase, $CDC2^{pThr\text{-}161}$ is dephosphorylated and remains in this state until mitosis is completed (Fig. 7, C–E).

We investigated whether CDKN3 is a CDC2 phosphatase. CDKN3 knockdown produces hyperphosphorylation of CDC2 at Thr-161 (Fig. 7 F), whereas CDC2 phosphorylation at Tyr-15, controlled by the CDC25 phosphatases (Gautier et al., 1991), is not affected by CDKN3 (Fig. 7 F) despite the spatial proximity of both phosphoresidues (Fig. 7 A). CDKN3 inactivates the CDC2–cyclin B kinase in an in vitro kinase assay (Fig. 7 G), and CDKN3-deficient cells fail to dephosphorylate $CDC2^{Thr\text{-}161}$ in early anaphase (Fig. 7 H). These findings indicate that CDKN3 dephosphorylates $CDC2^{pThr\text{-}161}$ in late mitosis. Because dephosphorylation of $CDC2^{pThr\text{-}161}$ may silence CDKs during the mitotic exit (Chan et al., 2008; Wu et al., 2009), the disrupted CDC2 activity in CDKN3-deficient cells may partially explain abnormal cell division resulting from loss of CDKN3.

Identification of candidate mitotic effectors of the CDKN3-CDC2 signaling axis

We used KinomeView technology (Cell Signaling Technology) to explore phosphosignatures of the key kinome branches upon CDKN3 knockdown in a Western blotting–based screen (Fig. S3, A–R; Zhang et al., 2002). Consistent with the role of CDKN3 in CDK regulation (Gyuris et al., 1993; Hannon et al., 1994), CDKN3 knockdown induced abnormalities in CDK signaling (Fig. S3 G). Next, we used the PhosphoScan proteomic platform (Cell Signaling Technology) to identify and quantify CDKN3-dependent CDK targets (Rush et al., 2005; Fig. 8 A). Many CDKN3 phosphotargets identified by this approach are known or hypothetical regulators of the mitotic spindle (Fig. S4 and Table S3), which was confirmed in silico by the g:Profiler tool (Eichhorn et al., 2012). We identified pSer-209 of the CKβ regulatory subunit as a target of CDKN3-CDC2. CK has been implicated in controlling multiple stages of cell division (Hériche et al., 1997; Litchfield et al., 1992; St-Denis and Litchfield, 2009). Therefore, we asked whether CKβ plays a role in the SAC.

First, we confirmed CDKN3-dependent phosphorylation of CKβ detected by mass spectrometry (Fig. 8 B) via Western blotting (Fig. 8 C). Total CKβ protein level was unaffected by CDKN3 knockdown (Fig. 8 C). We found that $CK\beta^{pSer\text{-}209}$ is enriched at centrosomes (Fig. 8 D), where CDKN3 and CDC2 colocalize during mitosis (Fig. 7 B). The $CK\beta^{pSer\text{-}209}$ signal appears at centrosomes in early mitosis and decreases in anaphase, but some $CK\beta^{pSer\text{-}209}$ is still found at telophase centrosomes (Fig. 8 E). The cell cycle–dependent change of the $CK\beta^{pSer\text{-}209}$ signal intensity (Fig. 8 E) parallels CDKN3-dependent dephosphorylation of $CDC2^{pThr\text{-}161}$ before mitotic exit (Fig. 7, C–E).

Next, we asked whether CKβ controls the SAC. CKβ knockdown reduced the percentage of taxol-treated cells arresting in mitosis (Fig. 8, F–H), confirming the role of CKβ in the SAC.

siRNA cells transfected with siRNA-sensitive GFP-CDKN3 construct (top). Transfection with either GFP-CDKN3 construct resulted in a similar level of GFP-CDKN3 expression in cells pretransfected with control siRNA (bottom two rows). (B) Quantification of the rescue experiment. Error bars indicate SEM. $n = 3$ experiments; $P < 0.0001$ in *t* test. (C) Validated siRNAs against CDKN3 recapitulate the SAC failure phenotype. (D) Quantification of the SAC failure phenotype induced by three CDKN3 siRNAs shown in C. $n = 9$, $P < 0.0001$ in one-way ANOVA. (E) Validation of CDKN3 knockdown by four separate siRNAs in quantitative Western blots. $n = 6$, $P < 0.0001$ in one-way ANOVA. Note the normal CDKN3 signal in cells transfected with MAD2 siRNA. (F) Cells transfected with four separate CDKN3 siRNAs express normal MAD2 level. The MAD2/actin ratio was quantified by Western blotting. $n = 6$, (not significant) n.s. in one-way ANOVA for each CDKN3 siRNA. Note the MAD2 knockdown ($P = 0.0025$) in cells transfected with positive control MAD2 siRNA. (G) Normal localization of endogenous MAD2 on prometaphase kinetochores in cells transfected with CDKN3 siRNAs. Note the lack of MAD2 signal in cells transfected with validated MAD2 siRNA. (H) Quantification of MAD2-positive prometaphase kinetochores in cells transfected with CDKN3 siRNAs and MAD2 siRNAs. $P < 0.0001$ in ANOVA, $n = 50$ 200-µm nuclear cross sections per siRNA. (I) MAD2 overexpression does not rescue the SAC failure phenotype induced by CDKN3 siRNA. Note the similar nuclear morphology of cells transfected with CDKN3 siRNA alone compared with CDKN3 siRNA followed by MAD2 overexpression. (J) The SAC failure in CDKN3 siRNA cells is not rescued by ectopic overexpression of MAD2. $n = 10$; n.s. in *t* test. (K) Expression of Flag-MAD2 in cells transfected with the construct used in rescue experiments (I and J).

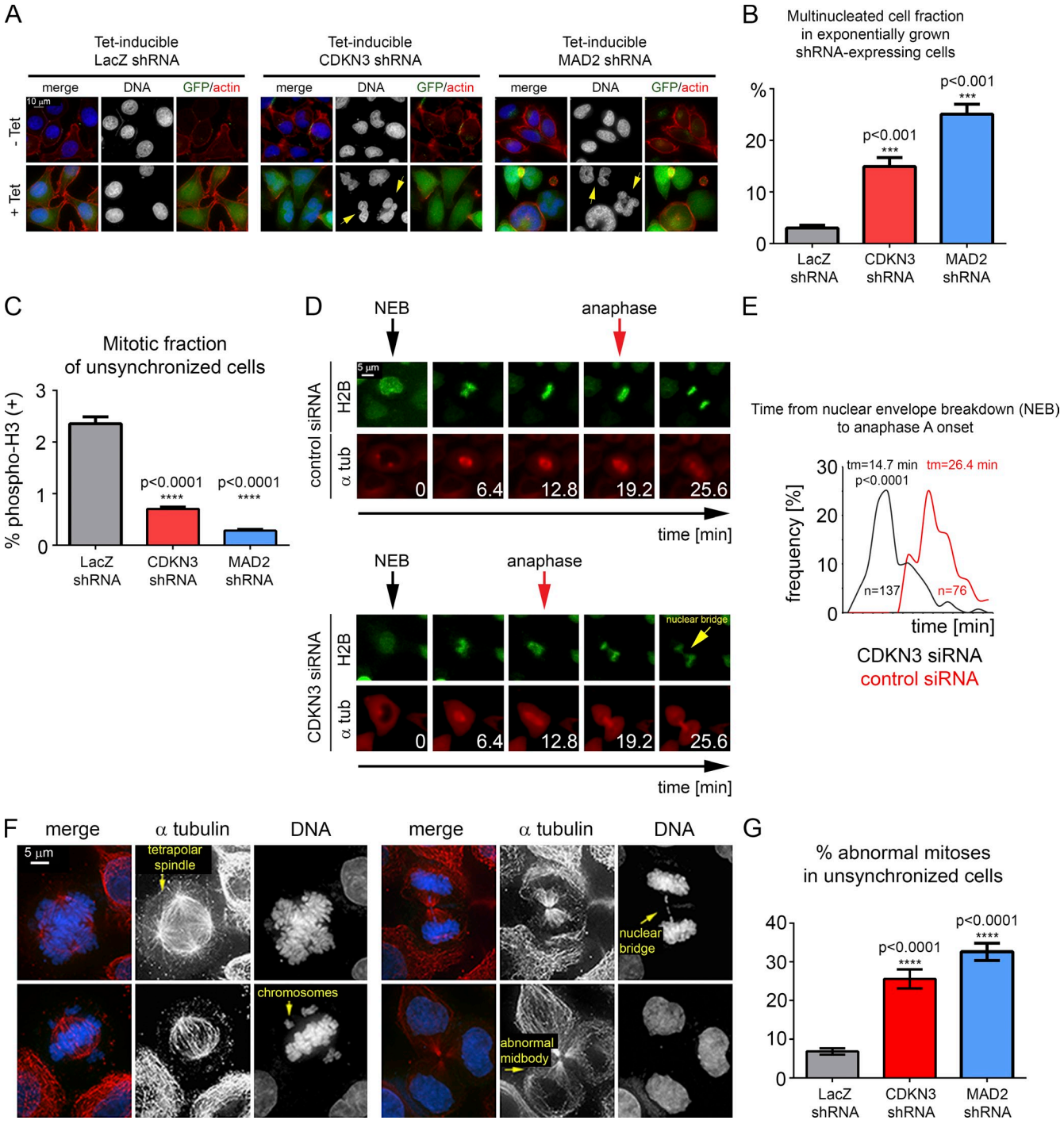

Figure 3. **CDKN3 is essential for normal mitosis.** (A) Inducible knockdown of CDKN3 and MAD2 leads to multinucleation (arrows, 200× magnification). (B) Quantification of multinucleation in CDKN3 and MAD2 knockout cells. $P < 0.0001$ for both CDKN3 and MAD2 siRNA (one-way ANOVA; $n = 5$). Error bars represent mean values ± SEM. (C) Knockdown of CDKN3 and MAD2 decreases mitotic index in unsynchronized cells as shown by flow cytometry. $P < 0.001$ in one-way ANOVA; $n = 6$. Error bars represent mean values ± SEM. (D) Representative time-lapse frames of cells dividing 72 h after transfection with negative control siRNA (A) and CDKN3 siRNA (B). Note the shortened time between NEB (black arrows) and anaphase (red arrows) upon CDKN3 knockdown. Time-lapse images were taken on an automated imaging system (Pathway 855; BD) in a controlled environment (5% CO_2, 37°C) every 192 s (3.2 min) using laser autofocus and a 20× NA 0.75 objective lens (Olympus); only every other frame from relevant sequences is shown for simplicity. (E) Frequency distributions of anaphase times. Movies of individual cells in unsynchronized populations were followed manually frame-by-frame to detect NEB. 76 control cells and 137 siCDKN3-transfected cells were measured in three independent experiments. $P < 0.0001$ in *t* test. (F) Gallery of mitotic cells transfected with CDKN3 siRNA. Note the multipolar spindles, unattached chromosomes, multinucleation, and cleavage furrows cutting through partially decondensed chromosomes. (G) Quantification of abnormal mitoses in unsynchronized CDKN3 and MAD2 knockout cells. $P < 0.0001$ (one-way ANOVA; $n = 5$). Error bars represent mean values ± SEM.

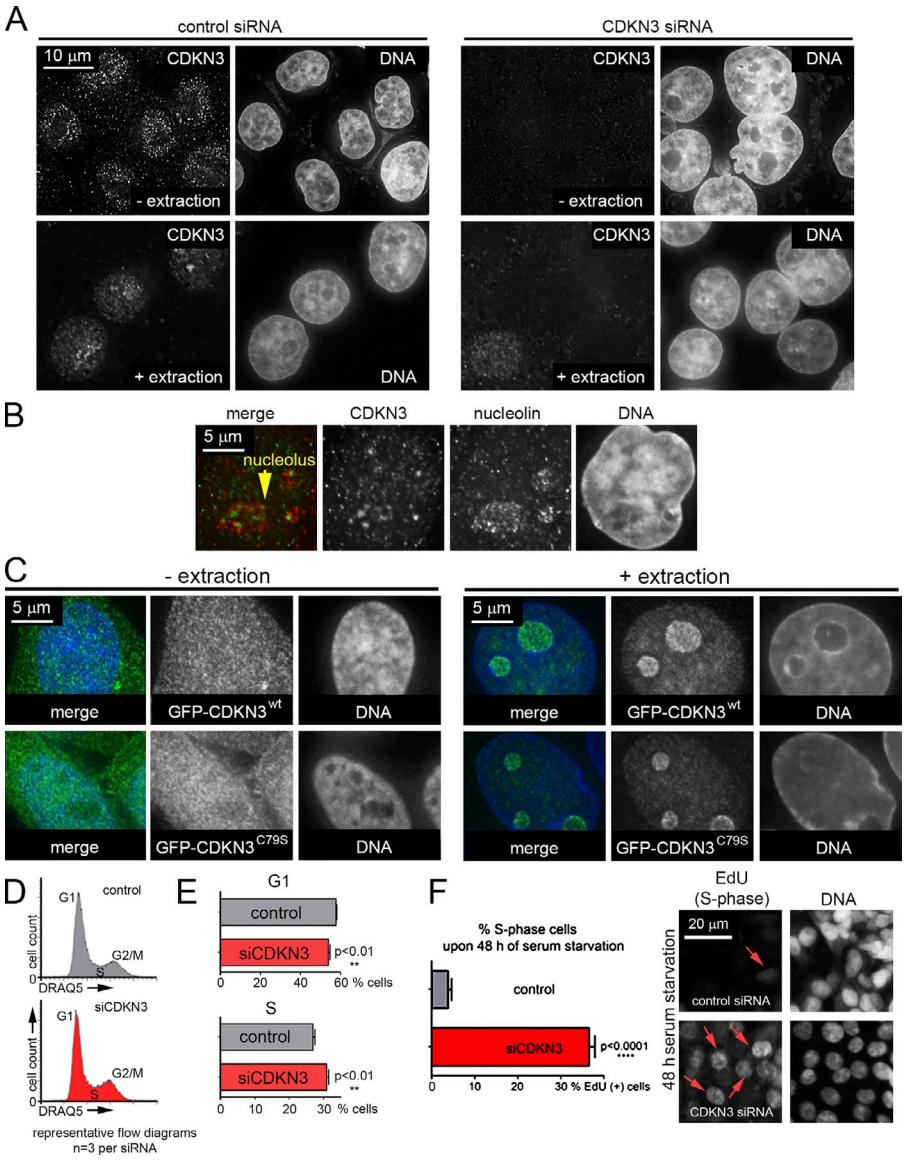

Figure 4. **CDKN3 is a nucleolar protein during interphase and controls G1/S transition.** (A) Endogenous CDKN3 localizes to interphase nuclei. Detergent extraction before fixation helps visualize the nucleolar fraction of endogenous CDKN3 (bottom). The signal is lost from cells transfected with CDKN3 siRNA (right), demonstrating antibody specificity. (B) Endogenous CDKN3 colocalizes with nucleolin. CDKN3 foci (green) are surrounded by diffuse nucleolin staining (red) in each nucleolus. (C) CDKN3 phosphatase activity is not required for subcellular targeting of GFP-CDKN3. HeLa cells were transfected with wild-type GFP-CDKN3 (top) and phosphatase-dead GFP-CDKN3^{C79S} point mutant (bottom). Nucleolar GFP-CDKN3 is visible in detergent-extracted nuclei. At least 100 nuclei were visualized per construct and condition. (D) Representative cell cycle profiles of cells transfected with control siRNA and CDKN3 siRNA. (E) Mildly increased S-phase fraction in HeLa cells transfected with CDKN3 siRNA. $P < 0.01$ in *t* test; $n = 4$. (F) CDKN3 is required for serum starvation–induced G1 arrest. Serum-starved HCT cells transfected with control and CDKN3 siRNAs were pulsed with EdU in serum-free medium to visualize cells that enter S phase (see micrographs on the right; red arrows indicate EdU-positive nuclei). $P < 0.0001$ in *t* test; $n = 4$.

These data indicate that loss of CDKN3 leads to global abnormalities in the human kinome signaling network, establish the role for CKβ in the SAC, and reveal that phosphorylation and subcellular localization of CKβ$^{pSer\text{-}209}$ are dynamically regulated as the cells divide.

Loss of CDKN3 and parallel activation of cyclin-dependent kinases in glioblastoma

Previous studies linking CDKN3 to cancer have generated conflicting evidence. CDKN3 was proposed to be overexpressed in some tumors (Lee et al., 2000; Lai et al., 2012) and lost in others (Yeh et al., 2000; Yu et al., 2007). In light of our findings, decreased expression of CDKN3 would be consistent with genomic instability and abnormal activation of CDKs, which are central features of GBM (Cancer Genome Atlas Research Network, 2008; Wiedemeyer et al., 2008, 2010). Therefore, we studied the CDKN3 expression in patient-derived GBM tumors.

We found that CDKN3 protein is ubiquitously expressed in healthy human brain (Fig. 9 A), and we observed decreased expression of CDKN3 in human GBMs (Fig. 9, B and C). We stained the same tumor panel with antibody against phosphorylated CDK targets to determine whether decreased CDKN3 is associated with elevated CDK activity in GBMs. Indeed, GBMs contained more cells with active CDKs than healthy brain (Fig. 9, D and E). Analysis of an independent cohort of patient-derived tumors (Fig. 9 F) confirmed decreased CDKN3 accompanied by elevated CDK activity in a fraction of GBMs (23%; $n = 26$; Fig. 9, G and H). The concordance between CDKN3 and phospho-CDK substrates was not absolute. Although all low-CDKN3 tumors are highly phospho-CDK–positive (e.g., Fig. 9 F, lane 1), some tumors expressing normal levels of CDKN3 have high phospho-CDK substrates (e.g., Fig. 9 F, lane 5). This may be explained by disruption of other CDK inhibitors (Wiedemeyer et al., 2008, 2010) or abnormal splicing of CDKN3 (Yu et al., 2007).

Discussion

Here, we combined functional genomics with phosphoproteomics to study the role of human phosphatases during mitosis. Our RNAi screen revealed four candidate spindle checkpoint

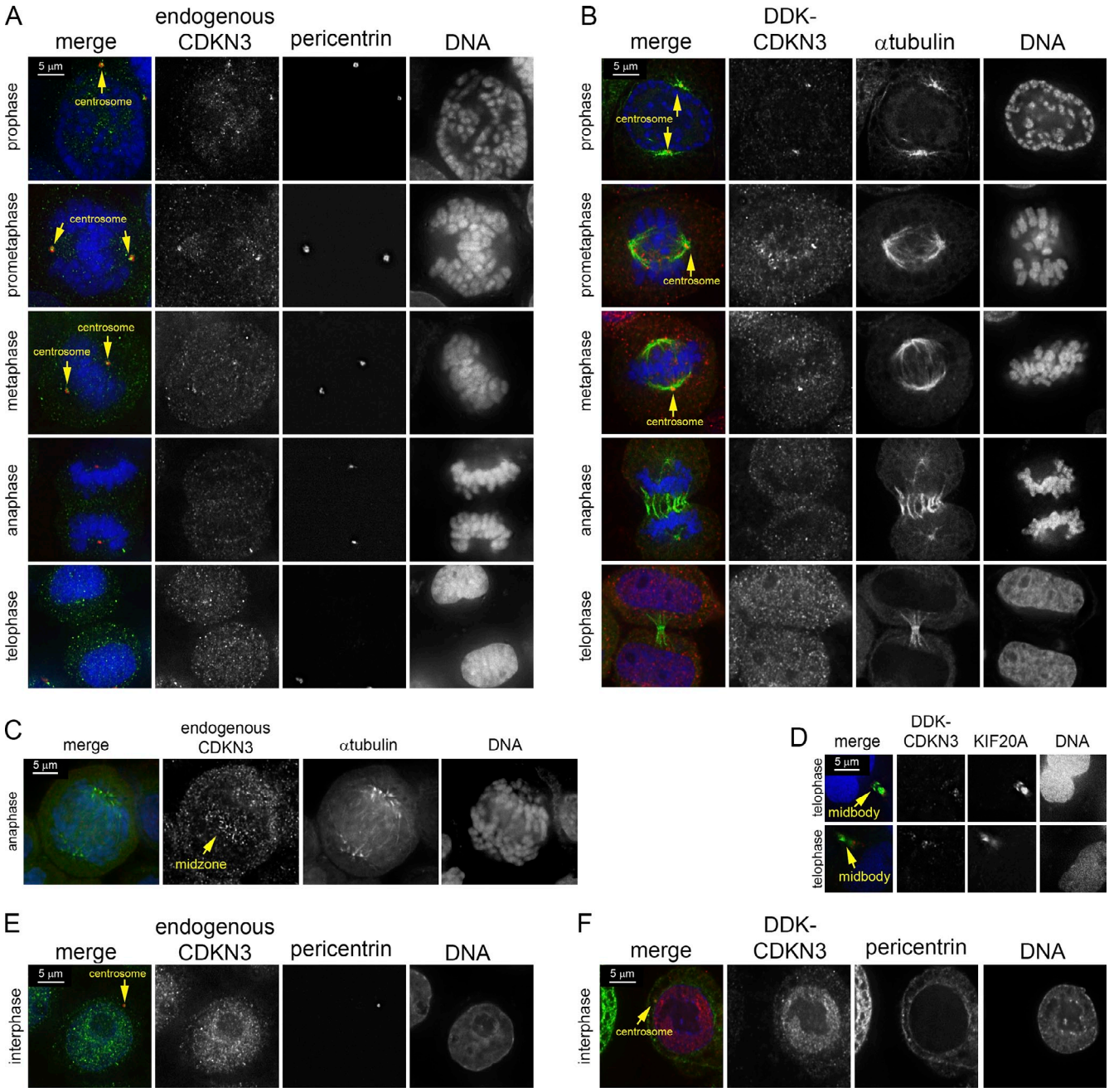

Figure 5. **CDKN3 localizes to centrosomes.** (A) Endogenous CDKN3 colocalizes with pericentrin during mitosis. (B) Stably overexpressed DDK-CDKN3 associates with centrosomes. (C) A small fraction of endogenous CDKN3 localizes to the midzone in anaphase. (D) Stably overexpressed DDK-CDKN3 colocalizes with KIF20A on midbodies in telophase. (E) A fraction of endogenous CDKN3 remains at centrosomes in interphase. (F) Localization of stably overexpressed DDK-CDKN3 to interphase centrosomes.

regulators: CDKN3, ANP32A (acidic nuclear phosphoprotein 32 family member), INPP5E (inositol polyphosphate-5-phosphatase), 5-NT (cytosolic 5-nucleotidase-II), and PP1M (protein phosphatase-1M). Additionally, the screen has rediscovered CDC25A as a mitotic entry gene (Lindqvist et al., 2009). These phosphatases belong to three major categories: (1) CDK regulators (CDKN3, ANP32A, and CDC25A), (2) phosphoinositol phosphatases (SAC-1 and INPP5E), and (3) nucleotide phosphatases (5-NT).

Further validation is necessary to confirm the mitotic function of SAC-1, INPP5E, ANP32A, and 5-NT (Hübner et al., 2010; Westhorpe et al., 2010). However, previous evidence allows us to speculate how these phosphatases may regulate mitosis. ANP32A may regulate PP2A (Habrukowich et al., 2010) to control the SAC via the PP2A–CDK pathway (Queralt et al., 2006; Schlaitz et al., 2007). The role of SAC-1 in stabilizing the spindle has been described previously (Liu et al., 2008). INPP5E has been linked to Joubert syndrome (MIM213200; Bielas et al., 2009; Jacoby et al., 2009), the genetic disease leading to abnormal brain morphogenesis (Wong et al., 1992). Intriguingly, germline mutations of another SAC protein, the kinetochore component LIS1, also led to abnormal brain development (Miller-Dieker

syndrome, MIM247200). It remains to be seen whether abnormal mitosis contributes to disease manifestations in Joubert syndrome. Finally, loss of 5-NT may disrupt the mitotic spindle–controlling Ran-GTP gradient (Clarke and Zhang, 2008). Overall, the candidate cell cycle regulators identified in our RNAi screen fit into the mitosis-orchestrating pathways (Fig. 10; Groigno and Whitaker, 1998; Queralt et al., 2006; Schlaitz et al., 2007; Clarke and Zhang, 2008).

We focused on dissecting the role of CDKN3 in regulating the human cell cycle. CDKN3 is essential for G1 arrest, in agreement with the known role of CDKN3 in inhibiting interphase CDKs (Gyuris et al., 1993; Hannon et al., 1994). The localization of CDKN3 is reminiscent of nucleolar sequestration of CDC14, the phosphatase that is released from nucleoli to inhibit CDKs at the mitotic exit in *Saccharomyces cerevisiae* (Visintin et al., 1998; Shou et al., 1999; Azzam et al., 2004). Mammalian cells contain sequence orthologues of CDC14, but the function of CDC14s is not conserved among eukaryotes (for review see Mocciaro and Schiebel, 2010). Some CDK-counteracting activities of CDKN3 during mitotic exit may overlap with *S. cerevisiae* CDC14.

We found that CDKN3 dephosphorylates CDC2$^{pThr\text{-}161}$ in late mitosis. Experiments in cell-free systems suggest that dephosphorylation of CDC2$^{pThr\text{-}161}$ may silence CDKs during the mitotic exit (Chan et al., 2008; Wu et al., 2009). Therefore, loss of CDKN3 may delay inactivation of CDKs in late mitosis. Consistently, we identified mitotic effectors whose CDK phosphorylation increases upon loss of CDKN3. We found the role of one of these phosphoproteins (CKβ) in the SAC, and observed that phospho-CKβ$^{Ser\text{-}209}$ localizes to centrosomes like its upstream regulators, CDKN3 and CDC2. Further research will reveal how the phosphorylation of other CDKN3-CDC2 targets (Table S3) regulates the mitotic exit. The candidate mitotic effectors of the CDKN3-CDC2 axis identified in our study include the cytokinesis regulator PRC1 (Neef et al., 2007), the microtubule/kinetochore regulator CLASP (Reis et al., 2009), and the KIF20A/MKLP2 kinesin (Hümmer and Mayer, 2009).

The dephosphorylation of CDC2$^{pThr\text{-}161}$ in CDKN3-deficient cells is delayed but not abolished. Because the PP2A phosphatase dephosphorylates the same residue (De Smedt et al., 2002), CDKN3 and PP2A may collaborate to silence CDKs at the mitotic exit (Fig. 10). PP2A is a tumor suppressor (Neviani et al., 2005; Rodriguez-Viciana et al., 2006; Sablina et al., 2007, 2010) essential for centrosome maintenance (Kotadia et al., 2008). Loss of CDKN3 also induces supernumerary centrosomes (Fig. 6). Therefore, CDKN3-deficient cells are at risk of aneuploidy not only due to the weakened SAC, but also because of the increased number of centrosomes.

CDKN3 protein expression is decreased in glioblastoma in parallel with activation of the CDKs. This finding enhances our understanding of the genomic instability in GBM. Loss of CDKN3 may promote carcinogenesis through several complementary mechanisms. First, weakened SAC leads to aneuploidy as discussed in the Introduction. Second, precise control of late-mitotic CDK activity prevents aneuploidy (for review see Tsichlis et al., 2007). Third, cells with supernumerary centrosomes develop aneuploidy due to abnormal chromosome segregation secondary to the increased frequency of merotelic kinetochore-spindle

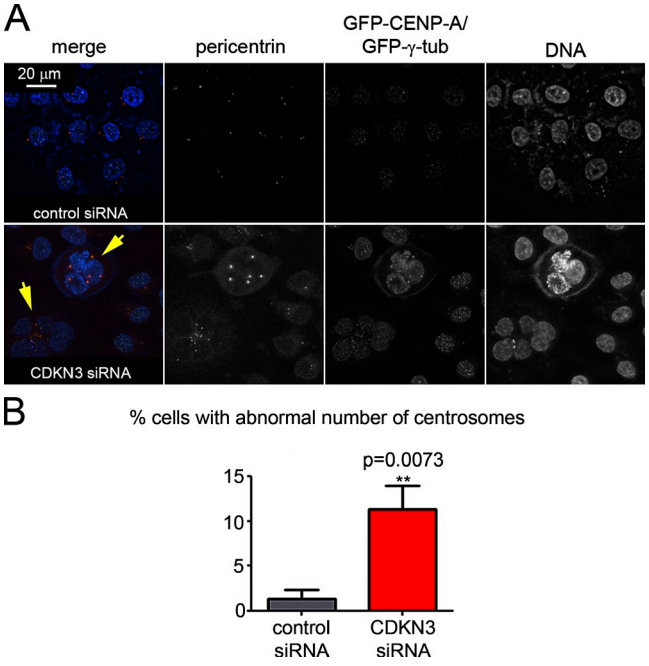

Figure 6. **CDKN3 is essential for centrosome maintenance.** (A) Abnormal centrosome clusters in HeLa$^{GFP\text{-}CENPA/GFP\text{-}\gamma\text{-}tub}$ cells transfected with CDKN3 siRNA. Endogenous pericentrin was visualized by immunofluorescence. Arrows indicate multinucleated cells with supernumerary centrosomes. (B) Loss of CDKN3 causes generation of supernumerary centrosomes. P = 0.0073 in *t* test; *n* = 5.

capture (Ganem et al., 2009). Fourth, loss of CDKN3 promotes micronucleation (Fig. 3, A and B). A recent elegant study revealed that micronuclei generated through abnormal mitosis accumulate double-stranded DNA breaks and undergo massive mutagenesis (Crasta et al., 2012). Further research will determine how these mechanisms contribute to genomic instability in CDKN3-deficient tumors.

The identification of abnormal activity of the CDKN3-CDC2 axis in glioblastoma provides experimental therapeutic opportunities. The CDKs can be targeted therapeutically (Manchado et al., 2010) in various tumors, including GBM (Wiedemeyer et al., 2010). We found that a pulse of a CDK inhibitor releases taxol-induced SAC arrest and induces multinucleation in human GBM cells (Fig. S5). Thus, this sequence of chemotherapeutics may work synergistically against tumors that have weakened SAC and activated CDKs. Also, CDKN3 or phospho-CDK substrate immunohistochemistry of tumor tissues (Fig. 9) may have diagnostic or prognostic importance.

In summary, our findings establish the role for CDKN3 in orchestrating mitosis through direct pathways (the SAC; timing of the mitotic clock) and indirect mechanisms (centrosome maintenance). This study provides mechanistic insights into the role of CDKN3 in carcinogenesis by proposing that CDKN3 functions as a tumor suppressor by preventing aneuploidy. These observations offer opportunities for anticancer drug development.

Materials and methods

Functional siRNA screen

The siRNA phosphatase library against a genome-wide set of phosphatases was purchased from Ambion. Cells were reverse-transfected with

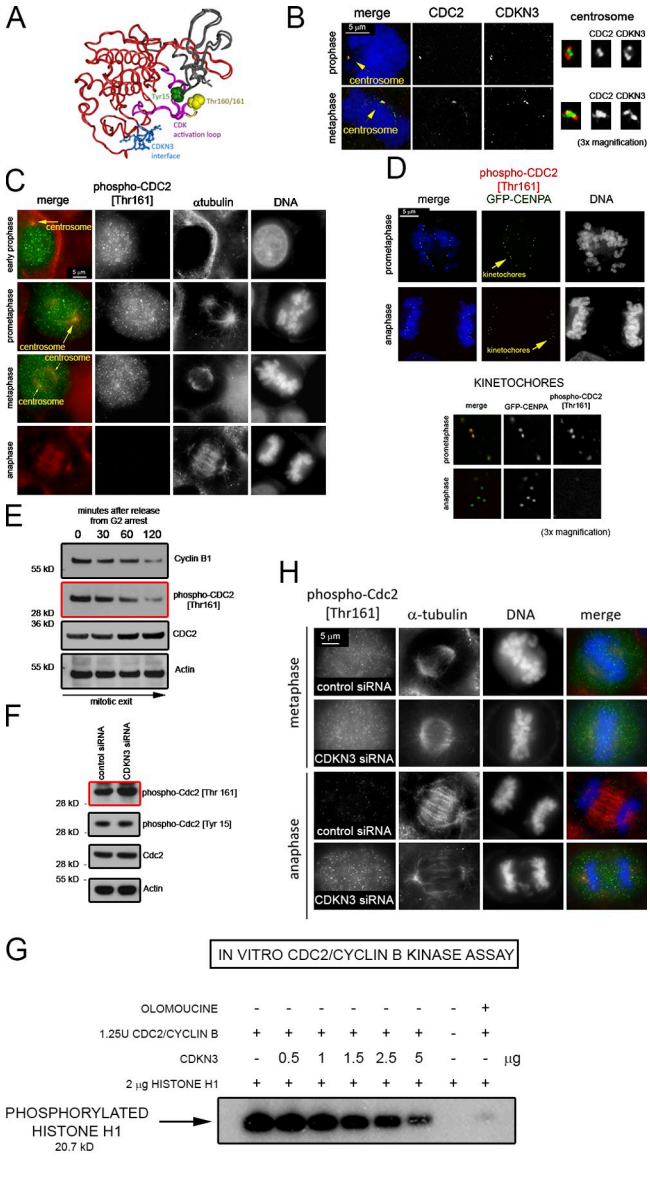

Figure 7. **CDKN3 modulates progression through mitosis via regulation of CDC2 phosphorylation at Thr-161.** (A) The CDKN3 interface is conserved in human CDK2 (Protein Database [PDB] accession no. 1B39) and CDC2 (PDB accession no. 3LFQ) kinases (GDSEID/DYK motifs, blue). Activation loops (magenta) include putative CDKN3 target residue (pThr160/161; yellow). CDC25 target sites are green. Regions of full conservation are red; other regions are gray. (B) Endogenous CDKN3 colocalizes with endogenous CDC2 on centrosomes during mitosis. (C) Endogenous CDC2^{pThr161} localizes to centrosomes and the mitotic spindle during cell division. Dephosphorylation of CDC2^{pThr161} occurs in anaphase. HeLa cells were stained with antibody recognizing CDC2$^{pThr-161}$, anti–α-tubulin antibody, and Hoechst 33342. (D) CDC^{pThr161} localizes to kinetochores in early mitosis. CDC2^{pThr161} (red) colocalizes with the kinetochore marker GFP-CENPA (green) in prometaphase but not in anaphase. (E) CDC2^{pThr161} is dephosphorylated at exit from mitosis. Cells were arrested in G2 through 24 h of exposure to RO3306 and washed to trigger mitotic entry. Decreasing cyclin B1 levels indicate cell cycle progression toward the mitotic exit. (F) Hyperphosphorylation of CDC2^{pThr161} in HeLa cells transfected with CDKN3 siRNA. Total CDC2 and CDC2^{pTyr15} levels are unaffected by CDKN3 siRNA. (G) Recombinant CDKN3 inactivates recombinant CDC2/cyclin B in an in vitro kinase assay in a dose-dependent manner. Increasing amounts of recombinant CDKN3 (0.5–5 μg) were incubated for 30 min in kinase buffer with a constant amount of active CDC2–cyclin B kinase complex, CDC2 substrate (histone H1), and radioactive [P^{32}]γ-ATP. CDC2-dependent H1 phosphorylation was detected by autoradiography. 150 mM olomoucine (a CDK kinase inhibitor) was used as a control. (H) Cells transfected with CDKN3 siRNA fail to dephosphorylate CDC2^{pThr161} in early anaphase. Note the normal CDC2$^{pThr-161}$ metaphase signal in control and CDKN3 siRNA cells. The CDC2$^{pThr-161}$ signal persists in CDKN3 siRNA cells during anaphase.

10 nM siRNA on 96-well plates (BD Falcon imaging microplates; 2,500 HeLa cells/well) using siPORT NeoFX transfection reagent (Applied Biosystems). 48 h later, cells were exposed to 100 nM taxol for 24 h and then fixed for visual inspection. Positive hits (defined as >20% nonmitotic cells after 24 h in 100 nM taxol) were verified in a HeLa/H2B-GFP/mCherry–α-tubulin cell line. To quantify CDKN3 and MAD2 protein levels in cells transfected with siRNAs against CDKN3 and MAD2, infrared fluorescence-based quantitative Western blotting was performed using secondary antibodies coupled to fluorescent dyes without enzymatic signal amplification (Odyssey CLX; LI-COR Biosciences).

Cell lines

HeLa cells stably expressing H2B-GFP/mCherry/α-tubulin and GFP-CENPA/γ-tubulin were gifts from C. Walczak (Indiana University, Bloomington, IN). HeLa cells were maintained in DMEM (Invitrogen) supplemented with 10% FBS and antibiotics. Neural progenitor cells isolated from postmortem human cortex, as described previously (Schwartz et al., 2003), were obtained directly from National Human Neural Stem Cell Resource, Children's Hospital of Orange County Research Institute (Orange, CA), and cultured according to published guidelines (Nethercott et al., 2007). Roscovitine was purchased from Selleck Chemicals. VS-83, taxol, and nocodazole were obtained from EMD Millipore. Olomoucine was purchased from Promega. Human glioblastoma cells were provided by K. Pollok (Indiana University School of Medicine, Indianapolis, IN).

Generation of inducible shRNA cell lines and CDKN3-expressing constructs

21-bp oligonucleotides targeting genes of interest were inserted into the pcDNA6/2-GW/EmGFP-miR vector (BLOCK-iT Pol II miR RNAi; Invitrogen). Successful insertion of oligonucleotides was confirmed by sequencing. Rapid BP/LR Gateway recombination was performed to transfer the miR-RNAi cassette into a tet-inducible pLENTI4/TO/V5-DEST lentiviral destination vector (ViraPower T-Rex; Invitrogen) using the pDONR221 vector (Invitrogen) as the intermediate. 293T cells were used to generate lentiviral particles. T-REx–HeLa cells (Invitrogen) were infected with miRNA lentiviruses, and cells were selected with zeocin (100 mg/ml). Zeocin-resistant colonies were expanded and tested for tetracycline-inducible target protein knockout and GFP expression by Western blotting.

The Myc-DDK–tagged CDKN3 construct was purchased from OriGene Technologies as the entry clone, verified by direct sequencing, and directly subcloned into pEGFP-C1 vector (Takara Bio Inc.) to generate the GFP fusion construct for immunofluorescence. The GFP-CDKN3 phosphatase-dead mutant (C79S) was generated through site-directed mutagenesis (Agilent Technologies) and verified by direct sequencing.

To generate a TAP-CDKN3-Myc-DDK–expressing construct, the CDKN3-Myc-DDK sequence was cloned into pNTAP-A vector (a gift of M. Harrington, Indiana University). To generate a stable TAP-CDKN3-Myc-DDK HeLa cell line for protein work and immunofluorescence, HeLa$^{GFP\text{-}H2B/mCherry\text{–}\alpha\text{-}tubulin}$ cells (a gift of C. Walczak) were transfected with this construct and selected with G418. Stable expression of the tagged CDKN3 protein of expected size was confirmed in G418-resistant clones by Western blotting.

Microscope image acquisition

Immunofluorescence microscopy. For imaging, HeLa cells were grown on ultrathin cover slides (Thermo Fisher Scientific) in DMEM (Invitrogen) supplemented with 10% FBS and antibiotics. Cells were fixed with ultrapure 4% paraformaldehyde (Electron Microscopy Sciences) in PBS for 10 min at room temperature. For routine immunostaining, cells were permeabilized with 0.1% Triton X-100 for 10 min, blocked with Image-iT FX signal enhancer (Invitrogen) or 1% bovine serum albumin in PBS for 30 min, and incubated with primary antibody for 2 h (DDK and pericentrin antibodies) or overnight (all other primary antibodies) on a shaker at room temperature. Cells were then washed with PBS, incubated with Alexa Fluor–conjugated secondary antibodies (Life Technologies) for 1 h, washed again, counterstained with Hoechst 33342 (Invitrogen) to visualize DNA, and mounted in SlowFade Light Antifade reagent (Molecular Probes). Images were taken at a room temperature on a deconvolution fluorescence microscope (personalDX DeltaVision; Applied Precision) fitted with a cooled

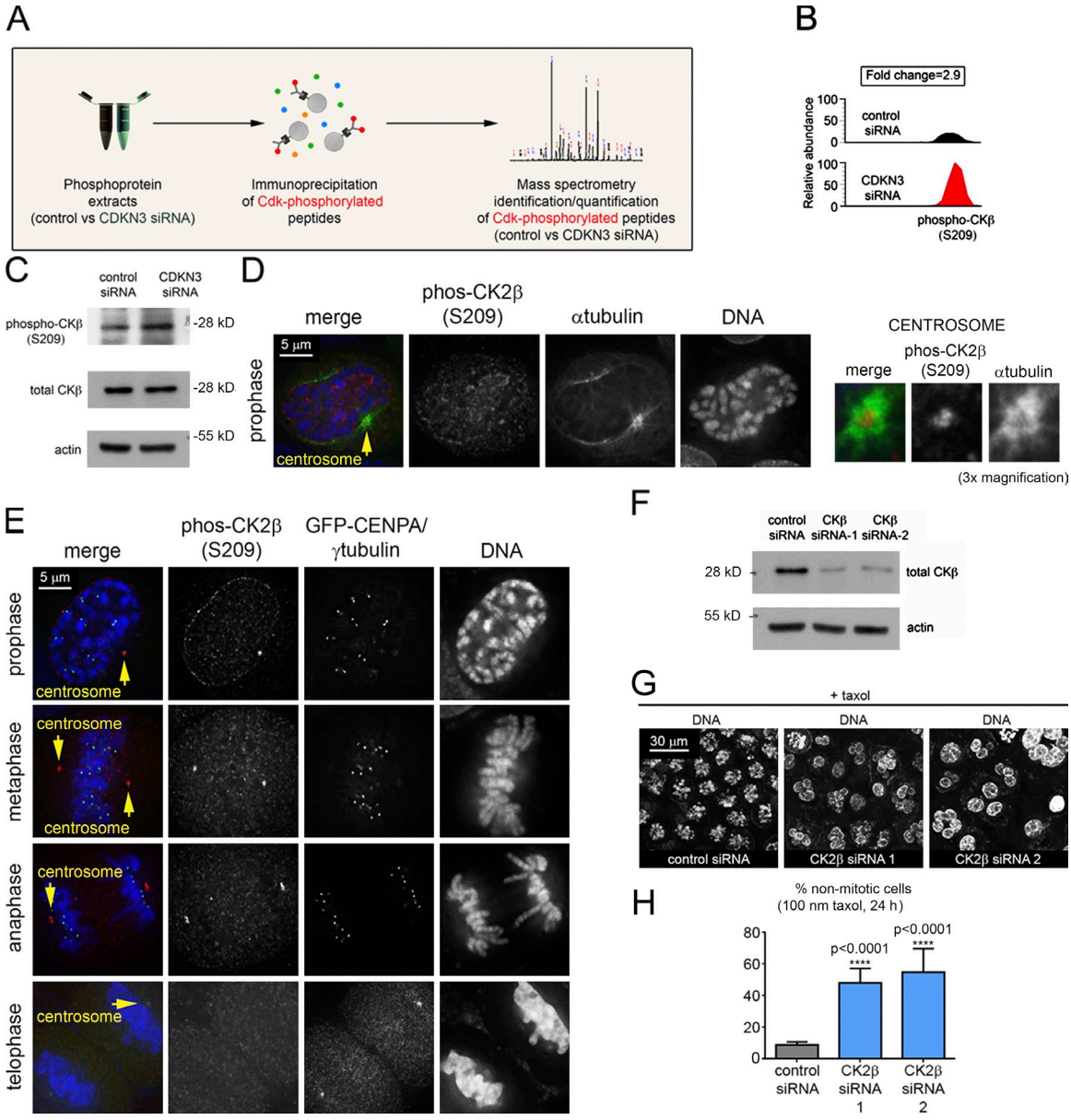

Figure 8. **A proteome-wide phospho-mass spectrometry screen identifies downstream mitotic effectors of CDKN3.** (A) Strategy to identify the CDKN3-CDC2 targets. (B) Mass spectrometry reveals hyperphosphorylation of CKβ$^{pSer\text{-}209}$ upon CDKN3 knockdown. Two samples per siRNA were analyzed in duplicate runs (with a total of four LC-MS/MS experiments); representative images are shown. (C) Western blot verification of proteomic screen. Note the increased phosphorylation of endogenous CKβ upon CDKN3 knockdown, whereas the total endogenous CKβ protein level remains the same. (D) Endogenous CKβ$^{pSer\text{-}209}$ localizes to centrosomes. (E) Endogenous CKβ$^{pSer\text{-}209}$ localizes to centrosomes throughout mitosis and disappears from centrosomes in telophase. (F) Western blot verification of CKβ knockdown. (G) CKβ is essential for mitotic spindle checkpoint. HeLa cells were transfected with CK2β siRNAs and treated with 100 nm taxol (24 h) 2 d after transfection. (H) Quantification of SAC failure resulting from CKβ knockdown. $P < 0.0001$ in one-way ANOVA; n = at least 5 counts per siRNA. Error bars represent mean values ± SEM.

CCD camera (CoolSNAP HQ2; Photometrics) and a SoftWoRx imaging software platform (Applied Precision). The following lenses were used: UPlan S-Apochromat 100× (NA 1.4), Plan-ApoN 60× (NA 1.42), and Uplan S-Apochromat 20× (NA 0.75; all from Olympus). The Applied Precision immersion oil objective lens (n = 1.516) was used with the 60× and 100× lenses. Images were acquired as a series of 100-nm- or 200-nm-thick z sections (for 60× and 100× lenses) or 1-μm-thick z sections (for the 20× lens). Deconvolution was performed with a SoftWoRx image workstation (ratio conservative, 10 iterations, noise filtering: medium; the same settings were used for all image stacks). Resulting images are presented as single transnuclear sections or collapsed image stacks. To generate scale bars, deconvolution image stacks were processed via the Imaris software platform. All images were collected and processed identically. For visualization of endogenous CDKN3 on centrosomes and in the nucleoli, cells were extracted with 0.1% Triton X-100 in PBS for 2 min before fixation with 4% paraformaldehyde to remove the diffuse nuclear and cytoplasmic protein fractions. The same extraction protocol was used to visualize CDKN3 colocalization with CDC2 on centrosomes, localization of CDC2$^{pThr\text{-}161}$ on kinetochores, and localization of overexpressed GFP-CDKN3 wild-type and phosphatase-dead fusion constructs on centrosomes and nucleoli. The primary MAD2 antibody used to visualize endogenous MAD2 on kinetochores was a gift of H. Yu (University of Texas Southwestern Medical Center, Dallas, TX). A list of primary antibodies used in this work is provided in Table S1.

Live cell imaging. For live imaging of dividing cells, cells were transfected with siRNAs in 96-well plates as described in the "Functional siRNA screen" section. Cells were grown in high-glucose DMEM without phenol red (Invitrogen) supplemented with 10% FBS and 1% pen-strep. Time-lapse images were taken on an automated high-throughput imaging system (Pathway 855;

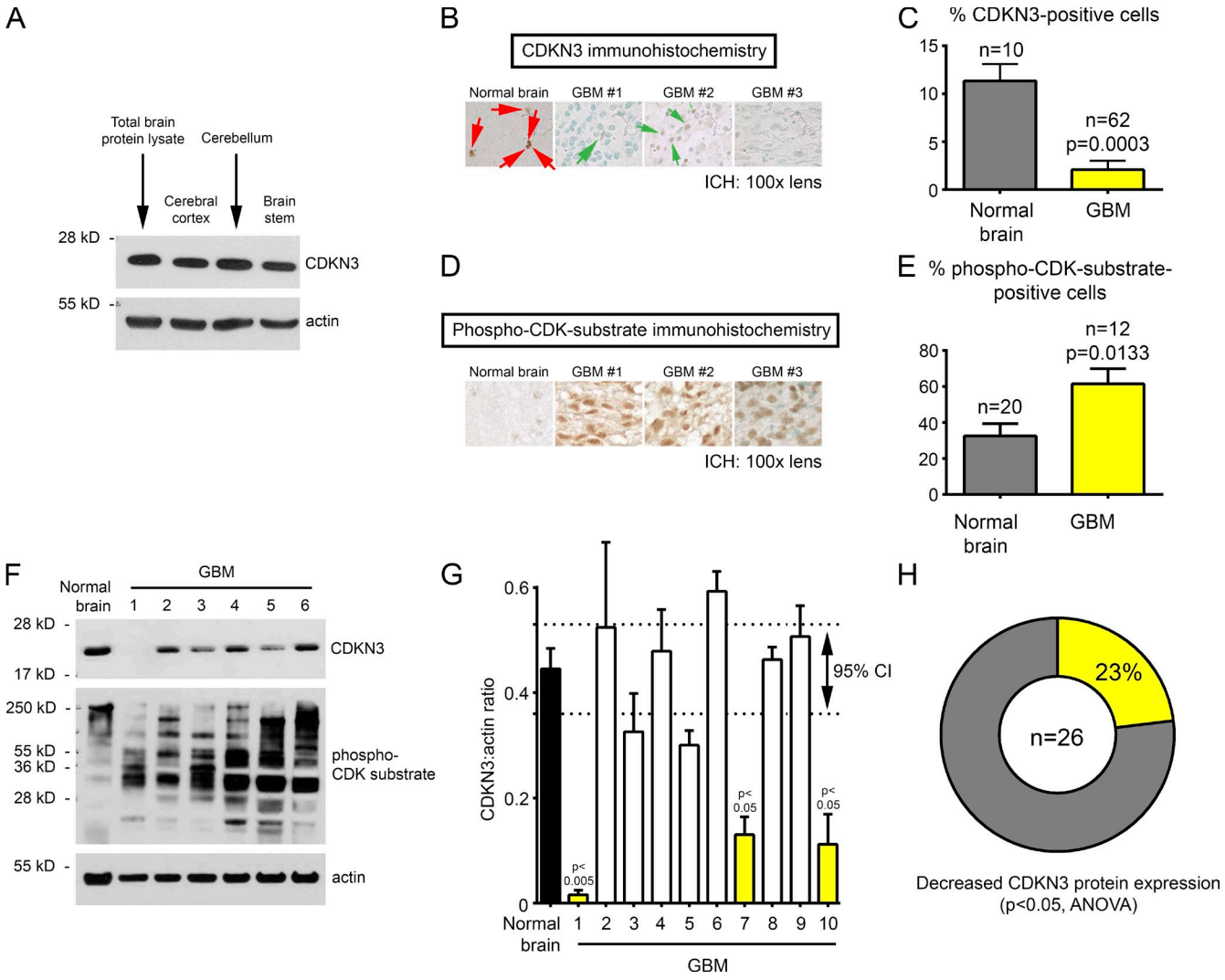

Figure 9. **Loss of CDKN3 expression and elevated CDK activity in glioblastoma.** (A) CDKN3 is ubiquitously expressed in human brain. (B) The CDKN3 protein is expressed in healthy brain (red arrows). CDKN3 expression is diminished (green arrows) in human GBM tumors. Images are shown at 100× magnification. (C) Immunohistochemistry quantification confirms loss of the CDKN3 protein in GBM. Percentages of CDKN3-positive cells in healthy brain cores and tumor specimens were compared by *t* test (P = 0.0003). Error bars represent mean values ± SEM. (D) Activation of CDKs in GBMs. Immunohistochemistry reveals increased CDK substrate phosphorylation in brain tumors compared with normal brain. (E) Quantification of increased CDK activity in GBMs. Percentages of phospho-CDK substrate–positive cells in healthy brain cores and tumors were compared by paired *t* test (P = 0.0133). Error bars represent mean values ± SEM. (F) Decreased expression of CDKN3 accompanied by CDK activation in an independent cohort of human GBMs. Note the increased phosphorylation of CDK substrates in all tumors. (G) Quantification of CDKN3 expression in healthy brain and GBM. CDKN3 and actin were quantified in at least three independent Westerns per specimen, and the ratios were compared with healthy brain (one-way ANOVA; *n* = 3 experiments for each tumor and 13 experiments for healthy brain). Yellow columns indicate tumors with significantly decreased total CDKN3 expression. Broken lines: 95% confidence interval. Error bars represent mean values ± SEM. (H) Quantification of the CDKN3 expression in 26 GBMs. 23% of tumors (6/26) showed significant loss of CDKN3 expression (one-way ANOVA; *n* = 3 experiments for each GBM and 13 experiments for healthy brain).

BD) every 192 s in an environmentally controlled chamber (5% CO_2, 37°C) (3.2 min) fitted with the Olympus 20× NA 0.75 lens. Laser autofocus was used to minimize photobleaching. The asynchronously growing cells were imaged for no longer than 4 h. Cells undergoing mitosis were identified on time-lapse movies and followed frame-by-frame to measure time between NEB and anaphase onset. NEB was defined as the dissolution of spherical nuclear shape and chromosome condensation, and anaphase onset was defined as the first frame showing separation of chromosomes toward spindle poles. 76 control cells and 137 siCDKN3-transfected cells were measured in three independent experiments. Attovision software (BD) was used for image acquisition. Photoshop (Adobe) and ImageJ software platforms were used to export movies. The Imaris software platform was used to generate still images shown on Fig. 3 to incorporate scale bars.

Cell cycle analysis, cell cycle synchronization, and flow cytometry

To synchronize cells in the G2 phase of the cell cycle for analysis of $CDC2^{pThr161}$ dephosphorylation at mitotic exit, cells were exposed to the CDC2 inhibitor RO3306 (final concentration of 9 mM; purchased from EMD Millipore; Vassilev et al., 2006) in growth medium for 24 h; G2 arrest was confirmed by flow cytometry. Cells were then released from the arrest by generous washing with RO3306-free growth medium, and cell lysates were collected at the indicated time points.

To synchronize HCT cells in G1 for the G1/S transition experiments, cells were serum-starved for 48 h, starting 24 h after siRNA transfection. For S-phase staining, HCT cells released from G1 arrest by exposure to FBS for 10 h, as described previously (Ye et al., 2003), were pulsed with 5-ethynyl-2′-deoxyuridine (EdU) for 1 h. A Click-iT EdU Assay (Invitrogen) was used to detect EdU-positive nuclei, and the percentage of EdU-positive S-phase nuclei was quantified manually under a deconvolution microscope. For flow cytometry, cells were fixed in 4% paraformaldehyde and permeabilized with 90% methanol before staining with phospho-histone-H3 antibody and DRAQ5 DNA stain (Cell Signaling Technology) to quantify mitotic cell fraction and obtain cell cycle profiles. Flow cytometry was performed on a FACSCalibur machine (BD).

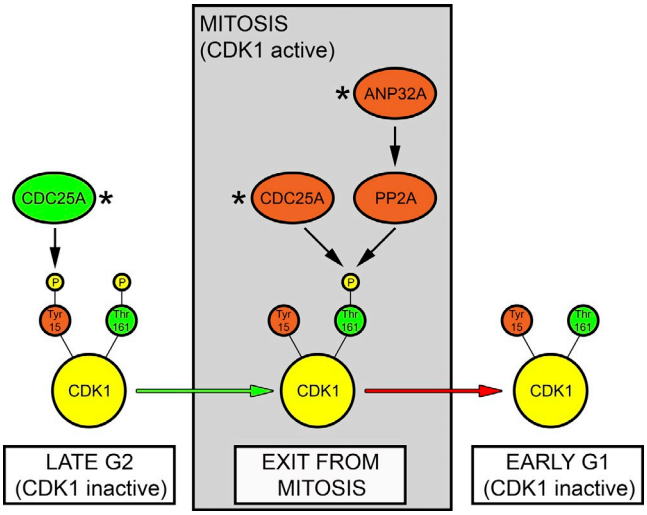

Figure 10. **Model of sequential CDC2 dephosphorylation during mitosis.** Phosphatases identified in this work are marked with asterisks. Dephosphorylation of Tyr-15 by CDC25 activates CDC2 at mitosis entry, whereas dephosphorylation of Thr-161 by CDKN3, PP2A, and other phosphatases guides CDC2 through late mitosis.

In vitro kinase assays

Radioactive in vitro CDK kinase assays were performed with recombinant CDC2–cyclin B kinase (New England Biolabs, Inc.) and recombinant CDKN3 produced in *Escherichia coli* (Cyclex). Indicated amounts of CDKN3 were incubated with 1.25 U CDC2/cyclin B and 2 µg CDC2 substrate (histone H1) in kinase buffer (50 mM Tris-HCl, pH 7.5, 10 mM $MgCl_2$, 1 mM EGTA, 2 mM DTT, 40 mM β-glycerophosphate, 20 mM p-nitrophenylphosphate, 0.1 mM sodium vanadate, and 0.01% Brij 35) for 30 min in the presence of radioactive [P^{32}]γ-ATP (1 µCi). Reactions were then terminated by adding SDS loading buffer, resolved by SDS-PAGE, and analyzed by autoradiography to detect CDC2-dependent in vitro phosphorylation of histone H1. Olomoucine (a small-molecule CDK kinase inhibitor used as a negative control) was purchased from Promega.

Proteomics sample preparation, mass spectrometry, and label-free protein quantification

For phospho-mass spectrometry analysis, cell pellets were flash-frozen in liquid nitrogen and sent on dry ice to Cell Signaling Technology for PhosphoScan analysis using the CDK Substrate Motif Antibody (Cell Signaling Technology catalogue no. 2324). Lysates were sonicated and centrifuged at 20,000 *g* for 15 min to remove insoluble material. The resulting "cleared" protein extracts were reduced with DTT and carboxamidomethylated with iodoacetamide. Normalization of total protein was performed for the lysates before trypsin digestion (catalogue no. LS003740; Worthington Biochemical Corporation), which was followed by solid-phase extraction of peptides with Sep-Pak C18 classical cartridges (catalogue no. WAT051910; Waters) and peptide lyophilization. Next, redissolved CDK-phosphorylated peptides were affinity-purified using CDK Substrate Motif antibody (Cell Signaling Technology). The peptides were subsequently released from antibody resin (0.15% trifluoroacetic acid, total volume = 100 µl) and subjected to duplicate liquid chromatography, mass spectrometry (LC-MS) analysis upon concentration with C18 spin tips. Peptides were then loaded onto a 10 cm × 75 µm capillary column (PicoFrit) packed with reversed-phase resin (Magic C18 AQ; Michrom Bioresources). Next, the column was developed with a 72-min linear gradient (acetonitrile in 0.125% formic acid) at 280 nL/min. Tandem mass spectra were collected with a hybrid mass spectrometer (LTQ-Orbitrap XL; Thermo Fisher Scientific) with a top 10 method, a dynamic exclusion repeat count of 1, and a repeat duration of 30 s. MS spectra were collected in the Orbitrap component of the mass spectrometer, and tandem mass spectrometry (MS/MS) spectra were collected in the LTQ. MS/MS spectra were evaluated using SEQUEST 3G and the SORCERER 2 platform from Sage-N Research (version 4.0; Lundgren et al., 2009). Peptide assignments were obtained using a 5% false-positive discovery rate. Searches were performed against the human National Center for Biotechnology Information database updated on 6 September 2010. Cysteine carboxamidomethylation was specified as a static modification, oxidation of methionine residues was allowed, and phosphorylation was allowed on serine, threonine, and tyrosine residues.

Parent ion intensities were derived from the samples' ion chromatogram files using proprietary software (Cell Signaling Technology) and used to generate quantitative data. Phosphopeptide-level differences between specimens were determined by calculating the ratios of raw intensities. Mean intensity values and raw ratios between specimens were computed based on raw phosphopeptide intensities in analyzed samples. Raw ratios were converted to $\log_2$ ratios and a median ratio was found for each comparison. The raw ratios were normalized based on the median ratio found, and normalized ratios and fold changes are reported. To make the quantification tables more complete, we used a proprietary computational program to search for phosphopeptide ions in the ion chromatogram files on the basis of their chromatographic retention times and their mass-to-charge (m/z) ratios for all phosphorylated peptides identified by MS/MS in at least one sample (Stokes et al., 2012). The retention time window used was variable and based on the pattern seen in the extracted ion chromatogram files, and the m/z range used was also variable and dependent on the mass error narrowing performed in a previous step. The computational program collected each peptide ion's retention time, observed m/z ratio, and intensity. Peak intensity measurements for many peptide ions were manually reviewed in the ion chromatogram files. This eliminated the possibility that the automated process selected the wrong chromatographic peak from which to derive the corresponding intensity measurement.

Samples to be used in the PhosphoScan study were also analyzed at Cell Signaling Technology using KinomeView (http://www.cellsignal.com/services/kinomeview.html), a Western blotting–based screen using all available phospho-motif antibodies. 20 mg of each sample was loaded on 4–20% Tris glycine gels, transferred to PVDF, blocked for 1 h at room temperature with 5% nonfat dry milk in TBS, and incubated overnight at 4°C in either 5% BSA in TBS/0.1% Tween 20 (TBS/T) or 5% nonfat dry milk in TBS/T as recommended by Cell Signaling Technology. Blots were washed three times for 5 min each in TBS/T and incubated with either anti–rabbit or anti–mouse DyLight 680 conjugate secondary antibody (catalogue Nos. 5366 and 5470, respectively; Cell Signaling Technology) for 1 h in 5% nonfat dry milk in TBS/T. Blots were washed again three times for 5 min with TBS/T, dried, and exposed in an Odyssey LI-COR near infrared imaging system.

Tumor immunohistochemistry and Western blotting

For analysis of CDKN3 expression in healthy human brain, fractionated human brain protein lysates were purchased from Takara Bio Inc. To study spindle checkpoint abnormalities in primary brain stem cells, primary cells from human brains isolated postmortem were obtained directly from National Human Neural Stem Cell Resource and cultured as described previously (Schwartz et al., 2003). For analysis of CDKN3 expression in human tumor specimens, a paraffin-embedded array of brain glioblastoma and normal tissue was purchased from Biomax (GL806a: 33 cases of brain glioblastoma, 5 cases of normal brain tissue, two tissue cores per case were mounted by the manufacturer on the same slice; GL1002: brain tumor/normal tissue array). The slides were deparaffinized in xylene (three changes) and hydrated with graded alcohols and distilled water. Antigen retrieval was performed in 0.4% pepsin buffer for 40 min at 37°C and followed by blocking of endogenous peroxidase activity with Peroxo-block (Invitrogen). After rinsing the slides in PBS, the slides were incubated with anti-CDKN3 antibody (ab72081, 1:100 dilution; Abcam) for 1 h. The antigen–antibody reaction was visualized by the avidin-biotin-peroxidase (Zymed Picture Plus kit; Invitrogen) with DAB (Vector Sk-4100) as the chromogen. The slide was counterstained with methyl green (BioVision) and then cleared in alcohol and xylene. The slide was mounted with Histomount (Invitrogen) and visualized with a microscope (Eclipse 80i; Nikon) equipped with a digital camera. The results were independently verified on another patient-derived brain tumor tissue array (T174; Biomax). Cell counting was performed in a double-blinded fashion by two independently working researchers (F.-C. Yang and S. Chen) who were not aware which tissue cores represent normal brain versus tumor tissue. Each tissue core was subdivided into 12 visual fields and cells were counted in four central fields per core. Results represent pooled mean and SEM values for normal brain tissue and GBM specimens. For Western blotting–based quantification of CDKN3 expression in glioblastomas, protein lysates of tumor specimens were subjected to Western blotting using antibodies against CDKN3 and actin at least thrice, and mean band intensity for each of the proteins was measured with ImageJ software. Results were analyzed with two-way analysis of variance (ANOVA).

Online supplemental material

Fig. S1 shows that a fraction of endogenous CDKN3 and overexpressed GFP-CDKN3 localizes to nucleoli. Fig. S2 shows that centrosomal localization

of CDKN3 does not depend on its phosphatase activity. Fig. S3 shows a kinome-wide screen for kinase pathway abnormalities resulting from CDKN3 knockdown. Fig. S4 shows that a quantitative kinome-wide phospho-mass spectrometry screen reveals candidate targets of the CDKN3-CDK signaling axis. Fig. S5 shows that CDK inhibition overcomes taxol-induced spindle checkpoint arrest in glioblastoma cells. Table S1 lists key antibodies used in this study. Table S2 lists siRNA sequences used to generate stable knockdown cell lines. Table S3 lists proteins differentially phosphorylated upon CDKN3 knockdown. Videos 1–6 show representative time-lapse movies showing abnormal mitoses in CDKN3 knockdown HeLa$^{GFP\text{-}H2B/mCherry\text{-}tubulin}$ cells in comparison to cells transfected with a negative control siRNA. Online supplemental material is available at http://www.jcb.org/cgi/content/full/jcb.201205125/DC1.

HeLa cells were gifts from Dr. Claire Walczak, and GBM cells were gifts from Dr. Karen Pollok. We thank Dr. Hongtao Yu for the MAD2 antibody used for immunofluorescence. We are grateful to Drs. Claire Walczak and Zhong-Yin Zhang (IU), and Dr. Xin Ye (Chinese Academy of Sciences, Beijing) for critical reading of the manuscript. We thank Cell Signaling Technology for the mass spectrometry experiments and data analysis. We wish to acknowledge Children's Hospital of Orange County (CHOC), National Human Neural Stem Cell Resource, and the CHOC Foundation for Children as the source of neuronal stem cells used in this study.

G. Nalepa was supported by a Morris Green Pediatric Research Fellowship, as well as a National Institutes of Health/National Center for Advancing Translational Sciences Award (KL2 TR000163), and the American Cancer Society (Institutional Research grant IRG-84-002-28). W. Clapp is supported by the National Institutes of Health (R01 CA155294-01, R01 CA74177-14, and R01-CA138237-04).

Submitted: 21 May 2012
Accepted: 20 May 2013

References

Azzam, R., S.L. Chen, W. Shou, A.S. Mah, G. Alexandru, K. Nasmyth, R.S. Annan, S.A. Carr, and R.J. Deshaies. 2004. Phosphorylation by cyclin B-Cdk underlies release of mitotic exit activator Cdc14 from the nucleolus. *Science*. 305:516–519. http://dx.doi.org/10.1126/science.1099402

Bielas, S.L., J.L. Silhavy, F. Brancati, M.V. Kisseleva, L. Al-Gazali, L. Sztriha, R.A. Bayoumi, M.S. Zaki, A. Abdel-Aleem, R.O. Rosti, et al. 2009. Mutations in INPP5E, encoding inositol polyphosphate-5-phosphatase E, link phosphatidyl inositol signaling to the ciliopathies. *Nat. Genet.* 41:1032–1036. http://dx.doi.org/10.1038/ng.423

Blenk, S., J. Engelmann, M. Weniger, J. Schultz, M. Dittrich, A. Rosenwald, H.K. Müller-Hermelink, T. Müller, and T. Dandekar. 2007. Germinal center B cell-like (GCB) and activated B cell-like (ABC) type of diffuse large B cell lymphoma (DLBCL): analysis of molecular predictors, signatures, cell cycle state and patient survival. *Cancer Inform.* 3:399–420.

Bouchoux, C., and F. Uhlmann. 2011. A quantitative model for ordered Cdk substrate dephosphorylation during mitotic exit. *Cell*. 147:803–814. http://dx.doi.org/10.1016/j.cell.2011.09.047

Burgess, A., S. Vigneron, E. Brioudes, J.C. Labbé, T. Lorca, and A. Castro. 2010. Loss of human Greatwall results in G2 arrest and multiple mitotic defects due to deregulation of the cyclin B-Cdc2/PP2A balance. *Proc. Natl. Acad. Sci. USA*. 107:12564–12569. http://dx.doi.org/10.1073/pnas.0914191107

Cahill, D.P., C. Lengauer, J. Yu, G.J. Riggins, J.K. Willson, S.D. Markowitz, K.W. Kinzler, and B. Vogelstein. 1998. Mutations of mitotic checkpoint genes in human cancers. *Nature*. 392:300–303. http://dx.doi.org/10.1038/32688

Cancer Genome Atlas Research Network. 2008. Comprehensive genomic characterization defines human glioblastoma genes and core pathways. *Nature*. 455:1061–1068. http://dx.doi.org/10.1038/nature07385

Chan, Y.W., H.T. Ma, W. Wong, C.C. Ho, K.F. On, and R.Y. Poon. 2008. CDK1 inhibitors antagonize the immediate apoptosis triggered by spindle disruption but promote apoptosis following the subsequent rereplication and abnormal mitosis. *Cell Cycle*. 7:1449–1461. http://dx.doi.org/10.4161/cc.7.10.5880

Clarke, P.R., and C. Zhang. 2008. Spatial and temporal coordination of mitosis by Ran GTPase. *Nat. Rev. Mol. Cell Biol.* 9:464–477. http://dx.doi.org/10.1038/nrm2410

Crasta, K., N.J. Ganem, R. Dagher, A.B. Lantermann, E.V. Ivanova, Y. Pan, L. Nezi, A. Protopopov, D. Chowdhury, and D. Pellman. 2012. DNA breaks and chromosome pulverization from errors in mitosis. *Nature*. 482:53–58. http://dx.doi.org/10.1038/nature10802

D'Angiolella, V., C. Mari, D. Nocera, L. Rametti, and D. Grieco. 2003. The spindle checkpoint requires cyclin-dependent kinase activity. *Genes Dev.* 17:2520–2525. http://dx.doi.org/10.1101/gad.267603

Dai, W., Q. Wang, T. Liu, M. Swamy, Y. Fang, S. Xie, R. Mahmood, Y.M. Yang, M. Xu, and C.V. Rao. 2004. Slippage of mitotic arrest and enhanced tumor development in mice with BubR1 haploinsufficiency. *Cancer Res.* 64:440–445. http://dx.doi.org/10.1158/0008-5472.CAN-03-3119

De Smedt, V., R. Poulhe, X. Cayla, F. Dessauge, A. Karaiskou, C. Jessus, and R. Ozon. 2002. Thr-161 phosphorylation of monomeric Cdc2. Regulation by protein phosphatase 2C in *Xenopus* oocytes. *J. Biol. Chem.* 277:28592–28600. http://dx.doi.org/10.1074/jbc.M202742200

De Souza, C.P., K.A. Ellem, and B.G. Gabrielli. 2000. Centrosomal and cytoplasmic Cdc2/cyclin B1 activation precedes nuclear mitotic events. *Exp. Cell Res.* 257:11–21. http://dx.doi.org/10.1006/excr.2000.4872

De Wulf, P., F. Montani, and R. Visintin. 2009. Protein phosphatases take the mitotic stage. *Curr. Opin. Cell Biol.* 21:806–815. http://dx.doi.org/10.1016/j.ceb.2009.08.003

Dobles, M., V. Liberal, M.L. Scott, R. Benezra, and P.K. Sorger. 2000. Chromosome missegregation and apoptosis in mice lacking the mitotic checkpoint protein Mad2. *Cell*. 101:635–645. http://dx.doi.org/10.1016/S0092-8674(00)80875-2

Eichhorn, P.J., L. Rodón, A. Gonzàlez-Juncà, A. Dirac, M. Gili, E. Martínez-Sáez, C. Aura, I. Barba, V. Peg, A. Prat, et al. 2012. USP15 stabilizes TGF-β receptor I and promotes oncogenesis through the activation of TGF-β signaling in glioblastoma. *Nat. Med.* 18:429–435. http://dx.doi.org/10.1038/nm.2619

Ganem, N.J., S.A. Godinho, and D. Pellman. 2009. A mechanism linking extra centrosomes to chromosomal instability. *Nature*. 460:278–282. http://dx.doi.org/10.1038/nature08136

Gautier, J., M.J. Solomon, R.N. Booher, J.F. Bazan, and M.W. Kirschner. 1991. cdc25 is a specific tyrosine phosphatase that directly activates p34cdc2. *Cell*. 67:197–211. http://dx.doi.org/10.1016/0092-8674(91)90583-K

Gharbi-Ayachi, A., J.C. Labbé, A. Burgess, S. Vigneron, J.M. Strub, E. Brioudes, A. Van-Dorsselaer, A. Castro, and T. Lorca. 2010. The substrate of Greatwall kinase, Arpp19, controls mitosis by inhibiting protein phosphatase 2A. *Science*. 330:1673–1677. http://dx.doi.org/10.1126/science.1197048

Gordon, D.J., B. Resio, and D. Pellman. 2012. Causes and consequences of aneuploidy in cancer. *Nat. Rev. Genet.* 13:189–203.

Groigno, L., and M. Whitaker. 1998. An anaphase calcium signal controls chromosome disjunction in early sea urchin embryos. *Cell*. 92:193–204. http://dx.doi.org/10.1016/S0092-8674(00)80914-9

Gyuris, J., E. Golemis, H. Chertkov, and R. Brent. 1993. Cdi1, a human G1 and S phase protein phosphatase that associates with Cdk2. *Cell*. 75:791–803. http://dx.doi.org/10.1016/0092-8674(93)90498-F

Habrukowich, C., D.K. Han, A. Le, K. Rezaul, W. Pan, M. Ghosh, Z. Li, K. Dodge-Kafka, X. Jiang, R. Bittman, and T. Hla. 2010. Sphingosine interaction with acidic leucine-rich nuclear phosphoprotein-32A (ANP32A) regulates PP2A activity and cyclooxygenase (COX)-2 expression in human endothelial cells. *J. Biol. Chem.* 285:26825–26831. http://dx.doi.org/10.1074/jbc.M110.147058

Hanahan, D., and R.A. Weinberg. 2011. Hallmarks of cancer: the next generation. *Cell*. 144:646–674. http://dx.doi.org/10.1016/j.cell.2011.02.013

Hanks, S., K. Coleman, S. Reid, A. Plaja, H. Firth, D. Fitzpatrick, A. Kidd, K. Méhes, R. Nash, N. Robin, et al. 2004. Constitutional aneuploidy and cancer predisposition caused by biallelic mutations in BUB1B. *Nat. Genet.* 36:1159–1161. http://dx.doi.org/10.1038/ng1449

Hannon, G.J., D. Casso, and D. Beach. 1994. KAP: a dual specificity phosphatase that interacts with cyclin-dependent kinases. *Proc. Natl. Acad. Sci. USA*. 91:1731–1735. http://dx.doi.org/10.1073/pnas.91.5.1731

Hériché, J.K., F. Lebrin, T. Rabilloud, D. Leroy, E.M. Chambaz, and Y. Goldberg. 1997. Regulation of protein phosphatase 2A by direct interaction with casein kinase 2alpha. *Science*. 276:952–955. http://dx.doi.org/10.1126/science.276.5314.952

Hoyt, M.A., L. Totis, and B.T. Roberts. 1991. *S. cerevisiae* genes required for cell cycle arrest in response to loss of microtubule function. *Cell*. 66:507–517. http://dx.doi.org/10.1016/0092-8674(81)90014-3

Hübner, N.C., L.H. Wang, M. Kaulich, P. Descombes, I. Poser, and E.A. Nigg. 2010. Re-examination of siRNA specificity questions role of PICH and Tao1 in the spindle checkpoint and identifies Mad2 as a sensitive target for small RNAs. *Chromosoma*. 119:149–165. http://dx.doi.org/10.1007/s00412-009-0244-2

Hümmer, S., and T.U. Mayer. 2009. Cdk1 negatively regulates midzone localization of the mitotic kinesin Mklp2 and the chromosomal passenger complex. *Curr. Biol.* 19:607–612. http://dx.doi.org/10.1016/j.cub.2009.02.046

Jacoby, M., J.J. Cox, S. Gayral, D.J. Hampshire, M. Ayub, M. Blockmans, E. Pernot, M.V. Kisseleva, P. Compère, S.N. Schiffmann, et al. 2009.

INPP5E mutations cause primary cilium signaling defects, ciliary instability and ciliopathies in human and mouse. *Nat. Genet.* 41:1027–1031. http://dx.doi.org/10.1038/ng.427

Jiang, R., Y. Xia, J. Li, L. Deng, L. Zhao, J. Shi, X. Wang, and B. Sun. 2010. High expression levels of IKKalpha and IKKbeta are necessary for the malignant properties of liver cancer. *Int. J. Cancer*. 126:1263–1274.

Kops, G.J., D.R. Foltz, and D.W. Cleveland. 2004. Lethality to human cancer cells through massive chromosome loss by inhibition of the mitotic checkpoint. *Proc. Natl. Acad. Sci. USA*. 101:8699–8704. http://dx.doi.org/10.1073/pnas.0401142101

Kotadia, S., L.R. Kao, S.A. Comerford, R.T. Jones, R.E. Hammer, and T.L. Megraw. 2008. PP2A-dependent disruption of centrosome replication and cytoskeleton organization in *Drosophila* by SV40 small tumor antigen. *Oncogene*. 27:6334–6346. http://dx.doi.org/10.1038/onc.2008.254

Lai, M.W., T.C. Chen, S.T. Pang, and C.T. Yeh. 2012. Overexpression of cyclin-dependent kinase-associated protein phosphatase enhances cell proliferation in renal cancer cells. *Urol. Oncol.* 30:871–878. http://dx.doi.org/10.1016/j.urolonc.2010.09.010

Lee, S.W., C.L. Reimer, L. Fang, M.L. Iruela-Arispe, and S.A. Aaronson. 2000. Overexpression of kinase-associated phosphatase (KAP) in breast and prostate cancer and inhibition of the transformed phenotype by antisense KAP expression. *Mol. Cell. Biol.* 20:1723–1732. http://dx.doi.org/10.1128/MCB.20.5.1723-1732.2000

Lee, S.H., F. McCormick, and H. Saya. 2010. Mad2 inhibits the mitotic kinesin MKlp2. *J. Cell Biol.* 191:1069–1077. http://dx.doi.org/10.1083/jcb.201003095

Li, R., and A.W. Murray. 1991. Feedback control of mitosis in budding yeast. *Cell*. 66:519–531. http://dx.doi.org/10.1016/0092-8674(81)90015-5

Lindqvist, A., V. Rodríguez-Bravo, and R.H. Medema. 2009. The decision to enter mitosis: feedback and redundancy in the mitotic entry network. *J. Cell Biol.* 185:193–202. http://dx.doi.org/10.1083/jcb.200812045

Litchfield, D.W., B. Lüscher, F.J. Lozeman, R.N. Eisenman, and E.G. Krebs. 1992. Phosphorylation of casein kinase II by p34cdc2 in vitro and at mitosis. *J. Biol. Chem.* 267:13943–13951.

Liu, Y., M. Boukhelifa, E. Tribble, E. Morin-Kensicki, A. Uetrecht, J.E. Bear, and V.A. Bankaitis. 2008. The Sac1 phosphoinositide phosphatase regulates Golgi membrane morphology and mitotic spindle organization in mammals. *Mol. Biol. Cell*. 19:3080–3096. http://dx.doi.org/10.1091/mbc.E07-12-1290

López-Avilés, S., O. Kapuy, B. Novák, and F. Uhlmann. 2009. Irreversibility of mitotic exit is the consequence of systems-level feedback. *Nature*. 459:592–595. http://dx.doi.org/10.1038/nature07984

Lorca, T., J.C. Labbé, A. Devault, D. Fesquet, J.P. Capony, J.C. Cavadore, F. Le Bouffant, and M. Dorée. 1992. Dephosphorylation of cdc2 on threonine 161 is required for cdc2 kinase inactivation and normal anaphase. *EMBO J.* 11:2381–2390.

Lundgren, D.H., H. Martinez, M.E. Wright, and D.K. Han. 2009. Protein identification using Sorcerer 2 and SEQUEST. *Curr. Protoc. Bioinformatics*. Chapter 13:13: 3.

Manchado, E., M. Guillamot, G. de Cárcer, M. Eguren, M. Trickey, I. García-Higuera, S. Moreno, H. Yamano, M. Cañamero, and M. Malumbres. 2010. Targeting mitotic exit leads to tumor regression in vivo: Modulation by Cdk1, Mastl, and the PP2A/B55α,δ phosphatase. *Cancer Cell*. 18:641–654. http://dx.doi.org/10.1016/j.ccr.2010.10.028

Mayer, T.U., T.M. Kapoor, S.J. Haggarty, R.W. King, S.L. Schreiber, and T.J. Mitchison. 1999. Small molecule inhibitor of mitotic spindle bipolarity identified in a phenotype-based screen. *Science*. 286:971–974. http://dx.doi.org/10.1126/science.286.5441.971

Meraldi, P., V.M. Draviam, and P.K. Sorger. 2004. Timing and checkpoints in the regulation of mitotic progression. *Dev. Cell*. 7:45–60. http://dx.doi.org/10.1016/j.devcel.2004.06.006

Michel, L.S., V. Liberal, A. Chatterjee, R. Kirchwegger, B. Pasche, W. Gerald, M. Dobles, P.K. Sorger, V.V. Murty, and R. Benezra. 2001. MAD2 haplo-insufficiency causes premature anaphase and chromosome instability in mammalian cells. *Nature*. 409:355–359. http://dx.doi.org/10.1038/35053094

Mir, S.E., P.C. De Witt Hamer, P.M. Krawczyk, L. Balaj, A. Claes, J.M. Niers, A.A. Van Tilborg, A.H. Zwinderman, D. Geerts, G.J. Kaspers, et al. 2010. In silico analysis of kinase expression identifies WEE1 as a gatekeeper against mitotic catastrophe in glioblastoma. *Cancer Cell*. 18:244–257. http://dx.doi.org/10.1016/j.ccr.2010.08.011

Mocciaro, A., and E. Schiebel. 2010. Cdc14: a highly conserved family of phosphatases with non-conserved functions? *J. Cell Sci.* 123:2867–2876. http://dx.doi.org/10.1242/jcs.074815

Mochida, S., S.L. Maslen, M. Skehel, and T. Hunt. 2010. Greatwall phosphorylates an inhibitor of protein phosphatase 2A that is essential for mitosis. *Science*. 330:1670–1673. http://dx.doi.org/10.1126/science.1195689

Musacchio, A., and E.D. Salmon. 2007. The spindle-assembly checkpoint in space and time. *Nat. Rev. Mol. Cell Biol.* 8:379–393. http://dx.doi.org/10.1038/nrm2163

Nalepa, G., M. Rolfe, and J.W. Harper. 2006. Drug discovery in the ubiquitin-proteasome system. *Nat. Rev. Drug Discov.* 5:596–613. http://dx.doi.org/10.1038/nrd2056

Neef, R., U. Gruneberg, R. Kopajtich, X. Li, E.A. Nigg, H. Sillje, and F.A. Barr. 2007. Choice of Plk1 docking partners during mitosis and cytokinesis is controlled by the activation state of Cdk1. *Nat. Cell Biol.* 9:436–444. http://dx.doi.org/10.1038/ncb1557

Nethercott, H., M. Sheridan, and P.H. Schwartz. 2007. Neural Stem Cell Culture. *In* Human Stem Cell Manual. J. Loring, editor. Academic Press, London. 311–333.

Neviani, P., R. Santhanam, R. Trotta, M. Notari, B.W. Blaser, S. Liu, H. Mao, J.S. Chang, A. Galietta, A. Uttam, et al. 2005. The tumor suppressor PP2A is functionally inactivated in blast crisis CML through the inhibitory activity of the BCR/ABL-regulated SET protein. *Cancer Cell*. 8:355–368. http://dx.doi.org/10.1016/j.ccr.2005.10.015

Niculescu, M.D., Y. Yamamuro, and S.H. Zeisel. 2004. Choline availability modulates human neuroblastoma cell proliferation and alters the methylation of the promoter region of the cyclin-dependent kinase inhibitor 3 gene. *J. Neurochem.* 89:1252–1259. http://dx.doi.org/10.1111/j.1471-4159.2004.02414.x

Ohba, S., K. Shimizu, S. Shibao, T. Miwa, T. Nakagawa, H. Sasaki, and H. Murakami. 2011. A glioblastoma arising from the attached region where a meningioma had been totally removed. *Neuropathology*. 31:606–611. http://dx.doi.org/10.1111/j.1440-1789.2011.01198.x

Padua, M.B., and P.J. Hansen. 2009. Changes in expression of cell-cycle-related genes in PC-3 prostate cancer cells caused by ovine uterine serpin. *J. Cell. Biochem.* 107:1182–1188. http://dx.doi.org/10.1002/jcb.22222

Parsons, D.W., S. Jones, X. Zhang, J.C. Lin, R.J. Leary, P. Angenendt, P. Mankoo, H. Carter, I.M. Siu, G.L. Gallia, et al. 2008. An integrated genomic analysis of human glioblastoma multiforme. *Science*. 321:1807–1812. http://dx.doi.org/10.1126/science.1164382

Poon, R.Y., and T. Hunter. 1995. Dephosphorylation of Cdk2 Thr160 by the cyclin-dependent kinase-interacting phosphatase KAP in the absence of cyclin. *Science*. 270:90–93. http://dx.doi.org/10.1126/science.270.5233.90

Queralt, E., C. Lehane, B. Novak, and F. Uhlmann. 2006. Downregulation of PP2A(Cdc55) phosphatase by separase initiates mitotic exit in budding yeast. *Cell*. 125:719–732. http://dx.doi.org/10.1016/j.cell.2006.03.038

Reis, R., T. Feijão, S. Gouveia, A.J. Pereira, I. Matos, P. Sampaio, H. Maiato, and C.E. Sunkel. 2009. Dynein and mast/orbit/CLASP have antagonistic roles in regulating kinetochore-microtubule plus-end dynamics. *J. Cell Sci.* 122:2543–2553. http://dx.doi.org/10.1242/jcs.044818

Rodriguez-Viciana, P., C. Collins, and M. Fried. 2006. Polyoma and SV40 proteins differentially regulate PP2A to activate distinct cellular signaling pathways involved in growth control. *Proc. Natl. Acad. Sci. USA*. 103:19290–19295. http://dx.doi.org/10.1073/pnas.0609343103

Rush, J., A. Moritz, K.A. Lee, A. Guo, V.L. Goss, E.J. Spek, H. Zhang, X.M. Zha, R.D. Polakiewicz, and M.J. Comb. 2005. Immunoaffinity profiling of tyrosine phosphorylation in cancer cells. *Nat. Biotechnol.* 23:94–101. http://dx.doi.org/10.1038/nbt1046

Sablina, A.A., W. Chen, J.D. Arroyo, L. Corral, M. Hector, S.E. Bulmer, J.A. DeCaprio, and W.C. Hahn. 2007. The tumor suppressor PP2A Abeta regulates the RalA GTPase. *Cell*. 129:969–982. http://dx.doi.org/10.1016/j.cell.2007.03.047

Sablina, A.A., M. Hector, N. Colpaert, and W.C. Hahn. 2010. Identification of PP2A complexes and pathways involved in cell transformation. *Cancer Res.* 70:10474–10484. http://dx.doi.org/10.1158/0008-5472.CAN-10-2855

Sawin, K.E., K. LeGuellec, M. Philippe, and T.J. Mitchison. 1992. Mitotic spindle organization by a plus-end-directed microtubule motor. *Nature*. 359:540–543. http://dx.doi.org/10.1038/359540a0

Schlaitz, A.L., M. Srayko, A. Dammermann, S. Quintin, N. Wielsch, I. MacLeod, Q. de Robillard, A. Zinke, J.R. Yates III, T. Müller-Reichert, et al. 2007. The *C. elegans* RSA complex localizes protein phosphatase 2A to centrosomes and regulates mitotic spindle assembly. *Cell*. 128:115–127. http://dx.doi.org/10.1016/j.cell.2006.10.050

Schmitz, M.H., M. Held, V. Janssens, J.R. Hutchins, O. Hudecz, E. Ivanova, J. Goris, L. Trinkle-Mulcahy, A.I. Lamond, I. Poser, et al. 2010. Live-cell imaging RNAi screen identifies PP2A-B55alpha and importin-beta1 as key mitotic exit regulators in human cells. *Nat. Cell Biol.* 12:886–893. http://dx.doi.org/10.1038/ncb2092

Schwartz, P.H., P.J. Bryant, T.J. Fuja, H. Su, D.K. O'Dowd, and H. Klassen. 2003. Isolation and characterization of neural progenitor cells from post-mortem human cortex. *J. Neurosci. Res.* 74:838–851. http://dx.doi.org/10.1002/jnr.10854

Shou, W., J.H. Seol, A. Shevchenko, C. Baskerville, D. Moazed, Z.W. Chen, J. Jang, A. Shevchenko, H. Charbonneau, and R.J. Deshaies. 1999. Exit

from mitosis is triggered by Tem1-dependent release of the protein phosphatase Cdc14 from nucleolar RENT complex. *Cell*. 97:233–244. http://dx.doi.org/10.1016/S0092-8674(00)80733-3

Sigoillot, F.D., S. Lyman, J.F. Huckins, B. Adamson, E. Chung, B. Quattrochi, and R.W. King. 2012. A bioinformatics method identifies prominent off-targeted transcripts in RNAi screens. *Nat. Methods*. 9:363–366. http://dx.doi.org/10.1038/nmeth.1898

Song, H., N. Hanlon, N.R. Brown, M.E. Noble, L.N. Johnson, and D. Barford. 2001. Phosphoprotein-protein interactions revealed by the crystal structure of kinase-associated phosphatase in complex with phosphoCDK2. *Mol. Cell*. 7:615–626. http://dx.doi.org/10.1016/S1097-2765(01)00208-8

Sotillo, R., E. Hernando, E. Díaz-Rodríguez, J. Teruya-Feldstein, C. Cordón-Cardo, S.W. Lowe, and R. Benezra. 2007. Mad2 overexpression promotes aneuploidy and tumorigenesis in mice. *Cancer Cell*. 11:9–23. http://dx.doi.org/10.1016/j.ccr.2006.10.019

Sotillo, R., J.M. Schvartzman, N.D. Socci, and R. Benezra. 2010. Mad2-induced chromosome instability leads to lung tumour relapse after oncogene withdrawal. *Nature*. 464:436–440. http://dx.doi.org/10.1038/nature08803

St-Denis, N.A., and D.W. Litchfield. 2009. Protein kinase CK2 in health and disease: From birth to death: the role of protein kinase CK2 in the regulation of cell proliferation and survival. *Cell. Mol. Life Sci.* 66:1817–1829. http://dx.doi.org/10.1007/s00018-009-9150-2

Stokes, M.P., C.L. Farnsworth, A. Moritz, J.C. Silva, X. Jia, K.A. Lee, A. Guo, R.D. Polakiewicz, and M.J. Comb. 2012. PTMScan direct: identification and quantification of peptides from critical signaling proteins by immunoaffinity enrichment coupled with LC-MS/MS. *Mol. Cell. Proteomics*. 11:187–201. http://dx.doi.org/10.1074/mcp.M111.015883

Stupp, R., W.P. Mason, M.J. van den Bent, M. Weller, B. Fisher, M.J. Taphoorn, K. Belanger, A.A. Brandes, C. Marosi, U. Bogdahn, et al. 2005. Radiotherapy plus concomitant and adjuvant temozolomide for glioblastoma. *N. Engl. J. Med.* 352:987–996. http://dx.doi.org/10.1056/NEJMoa043330

Sudakin, V., G.K. Chan, and T.J. Yen. 2001. Checkpoint inhibition of the APC/C in HeLa cells is mediated by a complex of BUBR1, BUB3, CDC20, and MAD2. *J. Cell Biol.* 154:925–936. http://dx.doi.org/10.1083/jcb.200102093

Tao, W., V.J. South, Y. Zhang, J.P. Davide, L. Farrell, N.E. Kohl, L. Sepp-Lorenzino, and R.B. Lobell. 2005. Induction of apoptosis by an inhibitor of the mitotic kinesin KSP requires both activation of the spindle assembly checkpoint and mitotic slippage. *Cancer Cell*. 8:49–59. http://dx.doi.org/10.1016/j.ccr.2005.06.003

Taylor, K.J., A.H. Sims, L. Liang, D. Faratian, M. Muir, G. Walker, B. Kuske, J.M. Dixon, D.A. Cameron, D.J. Harrison, and S.P. Langdon. 2010. Dynamic changes in gene expression in vivo predict prognosis of tamoxifen-treated patients with breast cancer. *Breast Cancer Res.* 12:R39. http://dx.doi.org/10.1186/bcr2593

Thompson, S.L., S.F. Bakhoum, and D.A. Compton. 2010. Mechanisms of chromosomal instability. *Curr. Biol.* 20:R285–R295. http://dx.doi.org/10.1016/j.cub.2010.01.034

Tsichlis, P.N., M. Hatziapostolou, and P.W. Hinds. 2007. Timing is everything: regulation of Cdk1 and aneuploidy. *Dev. Cell*. 12:477–479. http://dx.doi.org/10.1016/j.devcel.2007.03.010

Vassilev, L.T., C. Tovar, S. Chen, D. Knezevic, X. Zhao, H. Sun, D.C. Heimbrook, and L. Chen. 2006. Selective small-molecule inhibitor reveals critical mitotic functions of human CDK1. *Proc. Natl. Acad. Sci. USA*. 103:10660–10665. http://dx.doi.org/10.1073/pnas.0600447103

Visintin, R., K. Craig, E.S. Hwang, S. Prinz, M. Tyers, and A. Amon. 1998. The phosphatase Cdc14 triggers mitotic exit by reversal of Cdk-dependent phosphorylation. *Mol. Cell*. 2:709–718. http://dx.doi.org/10.1016/S1097-2765(00)80286-5

Westhorpe, F.G., M.A. Diez, M.D. Gurden, A. Tighe, and S.S. Taylor. 2010. Re-evaluating the role of Tao1 in the spindle checkpoint. *Chromosoma*. 119:371–379. http://dx.doi.org/10.1007/s00412-010-0261-1

Wiedemeyer, R., C. Brennan, T.P. Heffernan, Y. Xiao, J. Mahoney, A. Protopopov, H. Zheng, G. Bignell, F. Furnari, W.K. Cavenee, et al. 2008. Feedback circuit among INK4 tumor suppressors constrains human glioblastoma development. *Cancer Cell*. 13:355–364. http://dx.doi.org/10.1016/j.ccr.2008.02.010

Wiedemeyer, W.R., I.F. Dunn, S.N. Quayle, J. Zhang, M.G. Chheda, G.P. Dunn, L. Zhuang, J. Rosenbluh, S. Chen, Y. Xiao, et al. 2010. Pattern of retinoblastoma pathway inactivation dictates response to CDK4/6 inhibition in GBM. *Proc. Natl. Acad. Sci. USA*. 107:11501–11506. http://dx.doi.org/10.1073/pnas.1001613107

Wong, A.J., J.M. Ruppert, S.H. Bigner, C.H. Grzeschik, P.A. Humphrey, D.S. Bigner, and B. Vogelstein. 1992. Structural alterations of the epidermal growth factor receptor gene in human gliomas. *Proc. Natl. Acad. Sci. USA*. 89:2965–2969. http://dx.doi.org/10.1073/pnas.89.7.2965

Wu, J.Q., J.Y. Guo, W. Tang, C.S. Yang, C.D. Freel, C. Chen, A.C. Nairn, and S. Kornbluth. 2009. PP1-mediated dephosphorylation of phosphoproteins at mitotic exit is controlled by inhibitor-1 and PP1 phosphorylation. *Nat. Cell Biol.* 11:644–651. http://dx.doi.org/10.1038/ncb1871

Wurzenberger, C., and D.W. Gerlich. 2011. Phosphatases: providing safe passage through mitotic exit. *Nat. Rev. Mol. Cell Biol.* 12:469–482. http://dx.doi.org/10.1038/nrm3149

Ye, X., Y. Wei, G. Nalepa, and J.W. Harper. 2003. The cyclin E/Cdk2 substrate p220(NPAT) is required for S-phase entry, histone gene expression, and Cajal body maintenance in human somatic cells. *Mol. Cell. Biol.* 23:8586–8600. http://dx.doi.org/10.1128/MCB.23.23.8586-8600.2003

Yeh, C.T., S.C. Lu, T.C. Chen, C.Y. Peng, and Y.F. Liaw. 2000. Aberrant transcripts of the cyclin-dependent kinase-associated protein phosphatase in hepatocellular carcinoma. *Cancer Res.* 60:4697–4700.

Yu, Y., X. Jiang, B.S. Schoch, R.S. Carroll, P.M. Black, and M.D. Johnson. 2007. Aberrant splicing of cyclin-dependent kinase-associated protein phosphatase KAP increases proliferation and migration in glioblastoma. *Cancer Res.* 67:130–138. http://dx.doi.org/10.1158/0008-5472.CAN-06-2478

Zhang, H., X. Zha, Y. Tan, P.V. Hornbeck, A.J. Mastrangelo, D.R. Alessi, R.D. Polakiewicz, and M.J. Comb. 2002. Phosphoprotein analysis using antibodies broadly reactive against phosphorylated motifs. *J. Biol. Chem.* 277:39379–39387. http://dx.doi.org/10.1074/jbc.M206399200

Nalepa et al., http://www.jcb.org/cgi/content/full/jcb.201205125/DC1

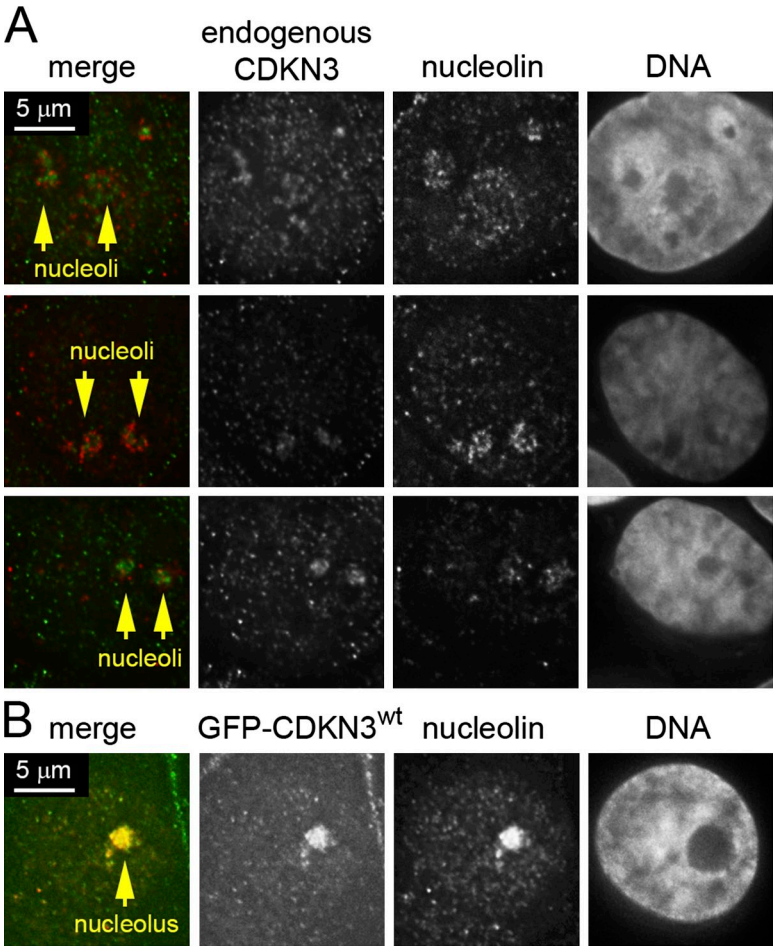

Figure S1. **A fraction of endogenous CDKN3 and overexpressed GFP-CDKN3 localizes to nucleoli.** (A) Three examples of extracted interphase cells to demonstrate localization of endogenous CDKN3 foci within the nucleolin clusters. (B) Overexpressed wild-type GFP-CDKN3 colocalizes with nucleolin in an extracted interphase nucleus (see also Fig. 4 C).

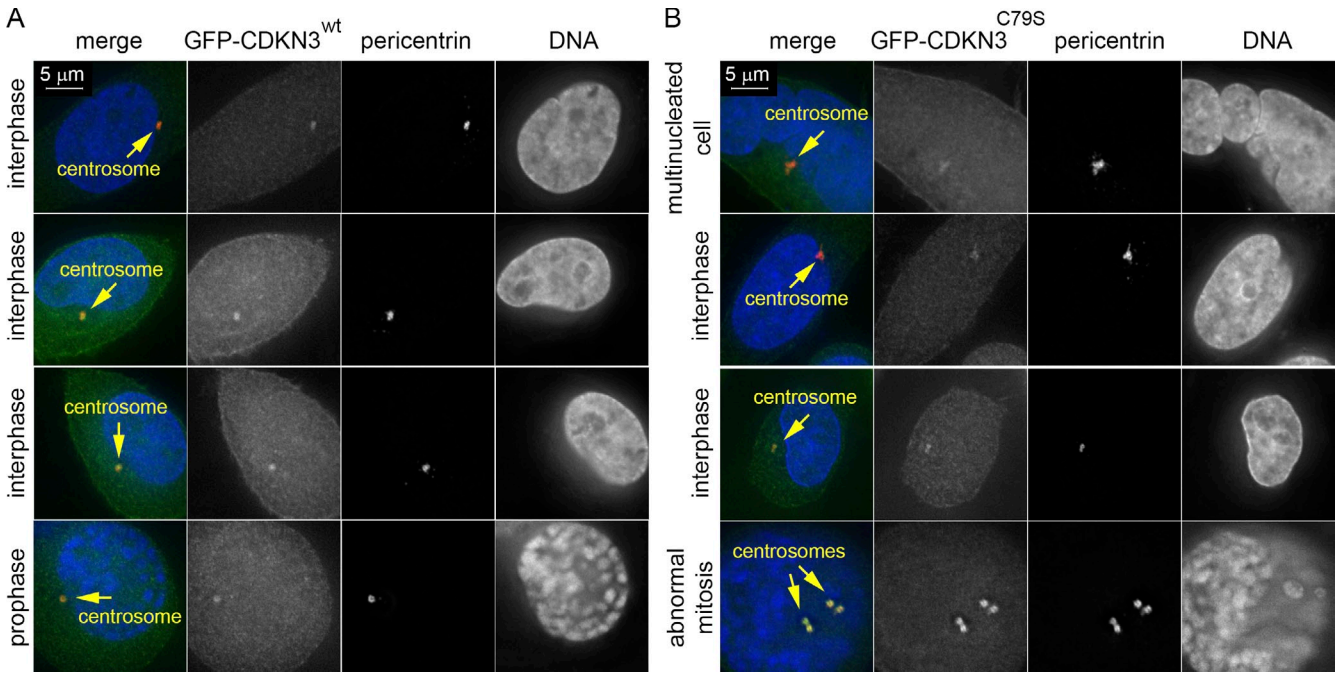

Figure S2. **Centrosomal localization of CDKN3 does not depend on its phosphatase activity.** Wild-type GFP-CDKN3 (A) and phosphatase-dead GFP-CDKN3 point mutant (B) localize to centrosomes, as shown by colocalization with the centrosomal marker pericentrin (red). Although both wild-type and phosphatase-dead GFP-CDKN3 fusion proteins localize to mitotic centrosomes (bottom), most cells grossly overexpressing GFP-CDKN3 constructs fail to enter mitosis and die, possibly because of interphase CDK inhibition by CDKN3 (Gyuris et al., 1993; Hannon et al., 1994).

A

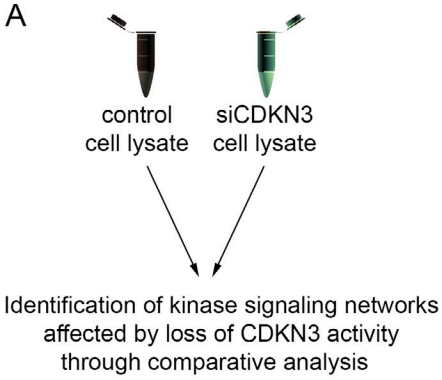

B

	Target	Recognized phosphosequence
1	AKT Substrate	RXX(s*/t*)
2	AKT Substrate	RXRXX(s*/t*)
3	ATM/ATR Substrate	(s*/t*)Q
4	ATM/ATR Substrate	(s*/t*)QG
5	CDK Substrate	(K/R)s*PX(K/R)
6	CK Substrate	t*(D/E)X(D/E)
7	MAPK Substrate	PXs*P
8	MAPK Substrate	PXt*P
9	PDK1 Docking Motif	(F/Y)(s*/t*)(F/Y)
10	PKA Substrate	(K/R)(K/R)X(s*t*)
11	PKC Substrate	(K/R)Xs*X(K/R)
12	PKD Substrate	LXRXX(s*/t*)
13	PLK Binding Motif	St*P
14	tP Motif	t*P, t*PP
15	tPE Motif	t*PE, t*P
16	tXR Motif	t*XR, t*PR

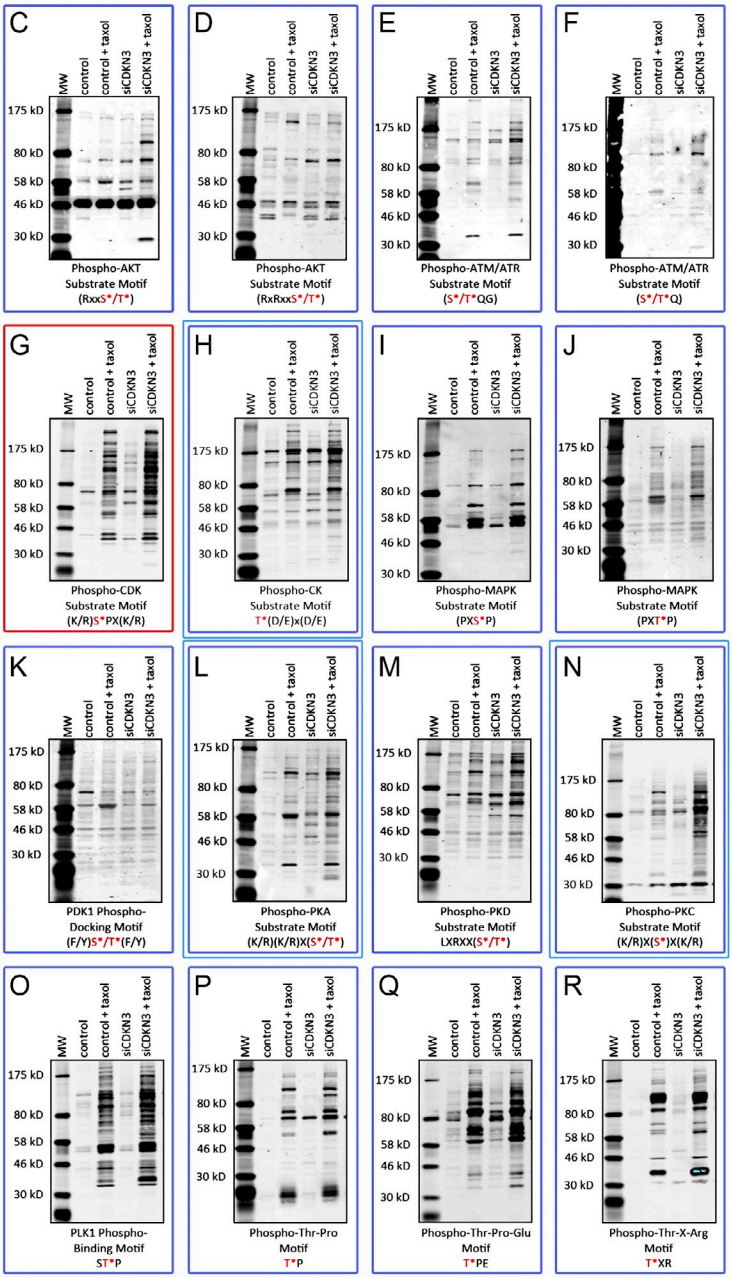

Figure S3. **Kinome-wide screen for kinase pathway signaling abnormalities resulting from CDKN3 knockdown.** (A) Screen schematic. The KinomeView analysis employs antibodies generated against consensus phosphorylation motifs in a Western blotting–based screen. Lysates of cultured cells transfected with control siRNA and CDKN3 siRNA (each with and without taxol) were resolved by SDS-PAGE in parallel and analyzed with the panel of phosphoantibodies. (B) List of sixteen phosphoantibodies used in the KinomeView analysis and their corresponding phosphomotifs. Phosphorylated serines (s) and threonines (t) are marked with asterisks and shown in red. (C–R) A kinome-wide screen reveals abnormal function of the CDK kinase branch in CDKN3 knockdown cells in the absence and presence of 24 h of exposure to 100 nM taxol. The phospho-CDK motif Western blot (G) is marked in red. The phospho-CK, phospho-PKA, and phospho-PKC substrate motif Western blots, which showed less significant changes than the phospho-CDK Western blot, are marked with double blue frames (H, L, and N).

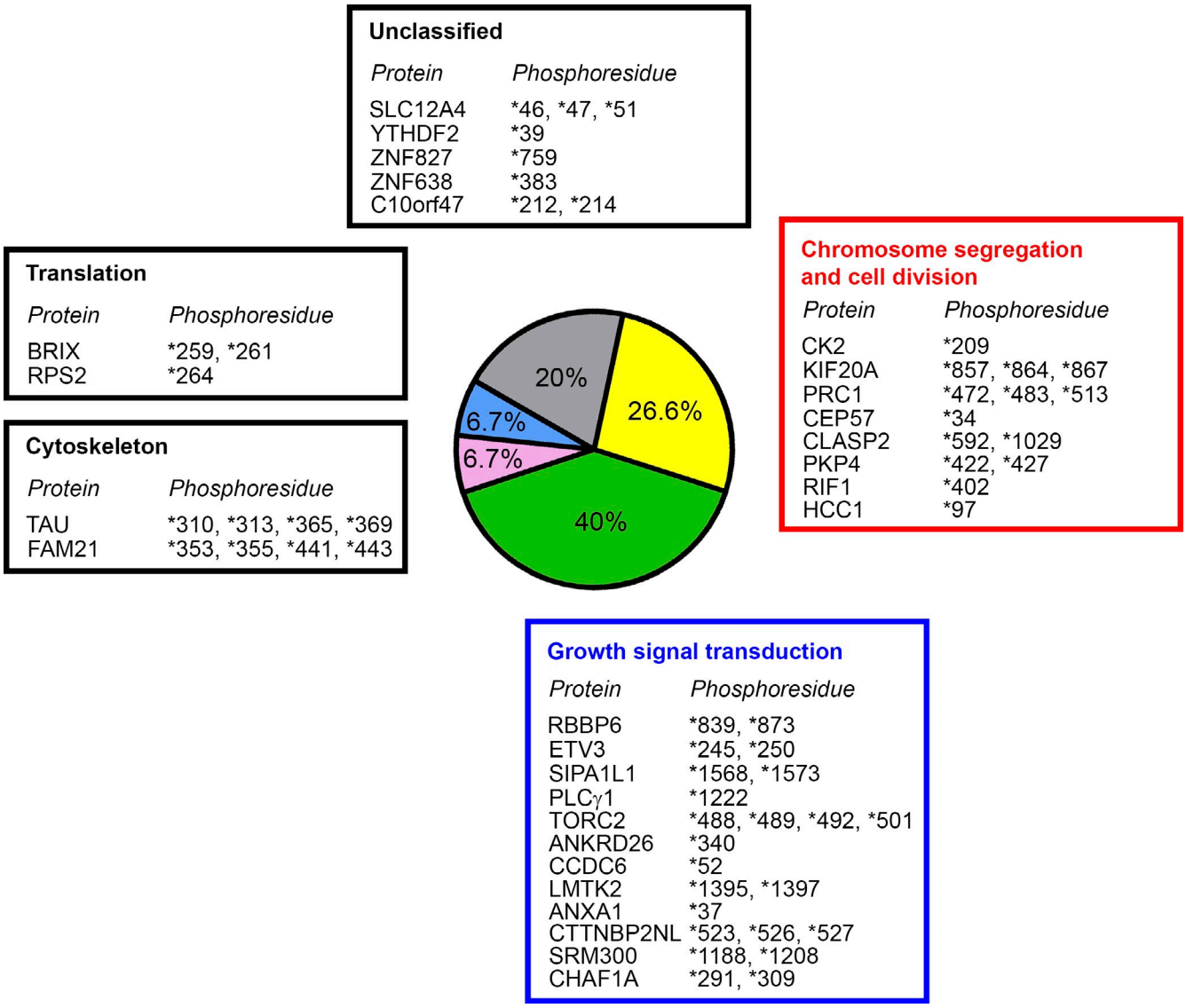

Figure S4. **A quantitative kinome-wide phospho-mass spectrometry screen reveals candidate targets of the CDKN3-CDK signaling axis.** Protease-digested protein extracts of HeLa cells transfected with control siRNA and CDKN3 siRNA were subjected to immunoaffinity purification using the CDK substrate motif antibody [(K/R)sPX(K/R)] followed by identification and quantitation of phosphopeptides by liquid chromatography, tandem mass spectrometry (LC-MS/MS; Rush et al., 2005). Note the targets involved in mitosis, chromosome segregation, and signal transduction. Affected phosphoresidues are marked with asterisks.

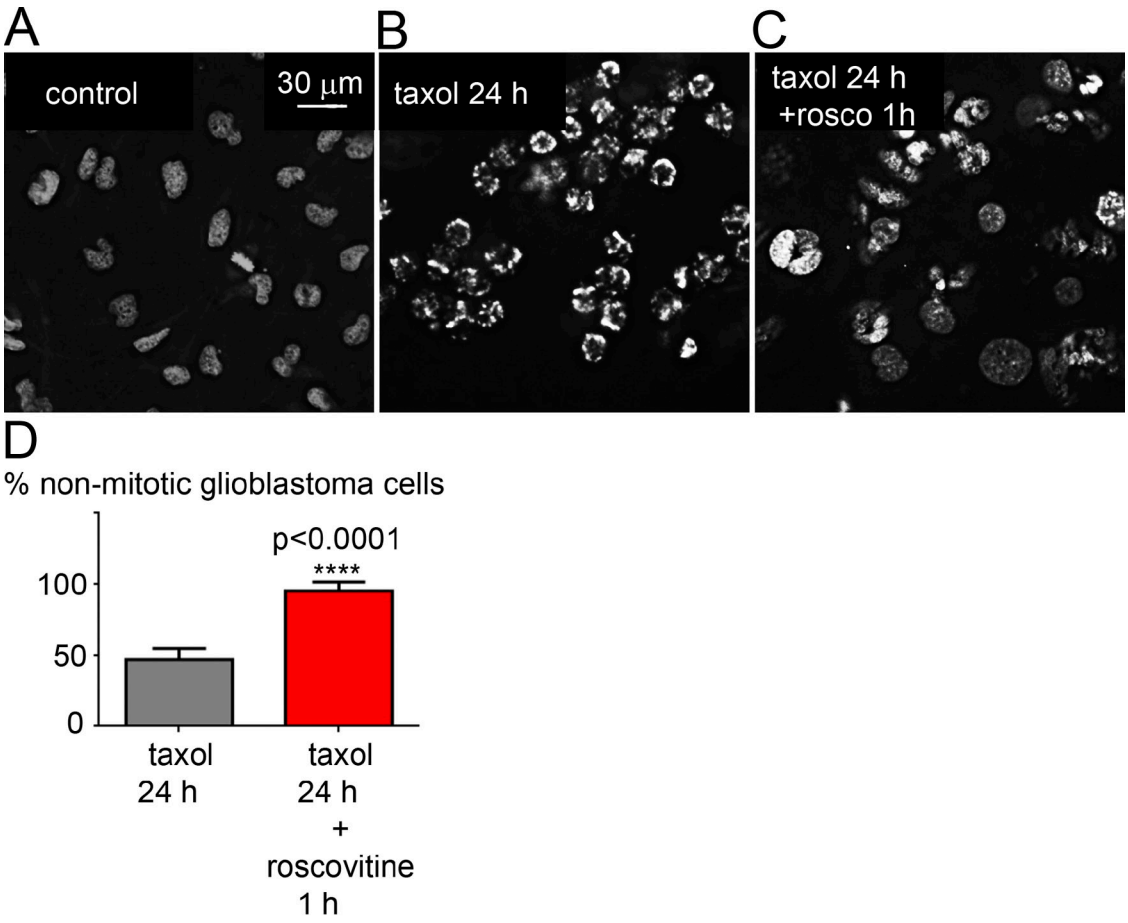

Figure S5. **CDK inhibition overcomes taxol-induced spindle checkpoint arrest in glioblastoma cells.** Human GBM-43 glioblastoma cells were exposed for 24 h to DMSO (A), 200 nM taxol (B), and 200 nM taxol followed by 1 h of treatment with 20 μm roscovitine (C). Note the partial mitotic arrest in cells treated with taxol alone (B) and multinucleation in cells sequentially treated with taxol and roscovitine (C). (D) Quantification of roscovitine-dependent spindle checkpoint release in GBM-43 glioblastoma cells. The percentage of nonmitotic cells is significantly higher in cells treated by taxol followed by roscovitine exposure, compared with taxol only ($P < 0.0001$, *t* test, $n = 5$).

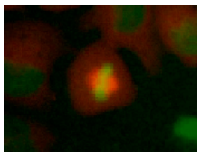

Video 1. **Representative HeLa cell stably expressing green histone H2B (GFP-H2B) and mCherry-tubulin undergoing normal mitosis.** The cell was imaged 72 h after transfection with negative-control siRNA. Images were acquired on an automated high-throughput fluorescence microscope (Pathway 855; BD) using BD imaging plates in a controlled environment (5% CO_2, 37°C). Frames were taken every 192 s (~3.2 min) for 2 h; only relevant frames are shown in the video.

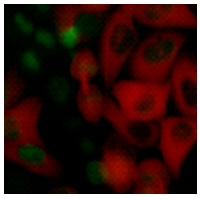

Video 2. **Accelerated mitosis in a HeLa$^{GFP\text{-}H2B/mCherry\text{-}tubulin}$ cell 72 h after CDKN3 siRNA transfection.** Note the immediate onset of chromosome segregation and cytokinesis without apparent chromosome congression. Images were acquired on an automated high-throughput fluorescence microscope (Pathway 855; BD) using BD imaging plates in a controlled environment (5% CO_2, 37°C). Frames were taken every 192 s (~3.2 min); only relevant frames are shown in the video.

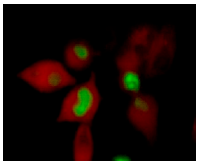

Video 3. **Abnormal mitosis in a binucleate HeLa cell stably expressing GFP-H2B and mCherry-tubulin.** Note the lack of synchrony between chromosome segregation and cytokinesis, and the cleavage furrow cutting through partially condensed chromosomes. The cell was imaged 72 h after transfection with siRNA targeting CDKN3. Images were acquired on an automated high-throughput fluorescence microscope (Pathway 855; BD) using BD imaging plates in a controlled environment (5% CO_2, 37°C). Frames were taken every 192 s (~3.2 min); only relevant frames are shown in the video.

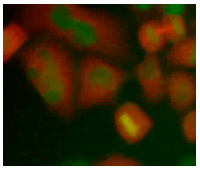

Video 4. **Abnormal mitosis in a mononuclear HeLa cell stably expressing GFP-H2B and mCherry-tubulin 72 h after transfection with CDKN3 siRNA.** Note the formation of a normal-appearing metaphase plate followed by abnormal cytokinesis, leading to generation of two cells that inherit an uneven amount of DNA. The cell attempts to generate a DNA-free cytoplasm bubble that is eventually retracted into one of two aneuploid daughter cells. Images were acquired on an automated high-throughput fluorescence microscope (Pathway 855; BD) using BD imaging plates in a controlled environment (5% CO_2, 37°C). Frames were taken every 192 s (~3.2 min); only relevant frames are shown in the video.

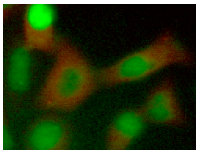

Video 5. **Abnormal cell division in a HeLa$^{H2B\text{-}GFP/mCherry\text{-}tubulin}$ cell 72 h after transfection with CDKN3 siRNA.** Note the apparent lack of chromosome congression and immediate onset of cytokinesis, with cleavage furrow pinching through partially condensed chromosomes, resulting in the generation of a nuclear bridge connecting two newborn cells. Images were acquired on an automated high-throughput fluorescence microscope using BD imaging plates (Pathway 855; BD) in a controlled environment (5% CO_2, 37°C). Frames were taken every 192 s (~3.2 min); only relevant frames are shown in the video.

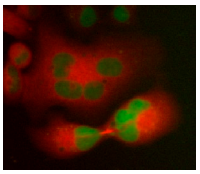

Video 6. **Abnormal cytokinesis in a HeLa cell stably expressing GFP-H2B and mCherry-tubulin 72 h after transfection with CDKN3 siRNA.** Two multinucleated daughter cells are connected by an abnormally thick midbody, which eventually undergoes retraction. This will presumably lead to generation of a giant multinucleated cell. Images were acquired on an automated high-throughput fluorescence microscope (Pathway 855; BD) using BD imaging plates in a controlled environment (5% CO_2, 37°C). Frames were taken every 192 s (~3.2 min); only relevant frames are shown in the video.

Table S1. **List of key primary antibodies used in this study**

Antibody	Supplier	Catalog No.	Application
Mouse anti–β-actin	Sigma-Aldrich	A-5441	WB
Mouse anti-Cdc2	Invitrogen	33-1800	WB, IF
Mouse anti-Cdc2	Cell Signaling Technology	9116	WB
Mouse mAb to Cyclin B1 (V152)	Cell Signaling Technology	4135	WB
Rabbit anti-Cdc25A	Cell Signaling Technology	3652	WB
Rabbit anti-GFP	Invitrogen	A11122	WB
Rabbit anti-Mad2	Abcam	ab97777	WB
Rabbit anti-Mad2	Santa Cruz Biotechnology, Inc.	sc-28261	WB
Rabbit anti-phospho-Cdc2 (Thr 161)	Cell Signaling Technology	9114	WB, IF
Rabbit anti-phospho-Cdc2 (Tyr15)	Cell Signaling Technology	9111	WB
Rabbit anti-phospho-histone H3	Cell Signaling Technology	9701	WB, IF
Rabbit anti-phospho-histone H3 (Alexa Fluor 555)	Cell Signaling Technology	3475	IF, FC
Rabbit polyclonal to CDKN3	Abcam	ab64974	WB, IF
Rabbit polyclonal to CDKN3	Abcam	ab32793	WB
Rabbit polyclonal to CDKN3	Abcam	ab72081	WB, ICH
Mouse monoclonal to CDKN3-m2H1	OriGene	TA503579	qWB
Mouse monoclonal to CDKN3-m2E11	OriGene	TA503580	qWB
Rabbit anti-Mad2	Yu laboratory	n/a	IF
CKβ antibody	Abcam	ab76025	WB
CKβ-phospho (S209) antibody	Abcam	ab59433	WB, IF
Rabbit anti-pericentrin	Abcam	ab4448	IF
Mouse anti-nucleolin	Invitrogen	39-6400	IF

For a list of antibodies used for kinome-wide screen, see Fig. S3. WB, Western blotting; qWB, quantitative Western blotting; IF, immunofluorescence; ICH, immunohistochemistry; FC, flow cytometry.

Table S2. **List of siRNA sequences used to generate stable knockdown cell lines**

Gene	siRNA sequence
LacZ	3′-AAATCGCTGATTTGTGTAGTC-5′
CDKN3	3′-GAATTGGAGTCTGTTCATCTT-5′
MAD2L1	3′-ATTGGAAACTGATTCAATAGG-5′

References

Gyuris, J., E. Golemis, H. Chertkov, and R. Brent. 1993. Cdi1, a human G1 and S phase protein phosphatase that associates with Cdk2. *Cell*. 75:791–803. http://dx.doi.org/10.1016/0092-8674(93)90498-F

Hannon, G.J., D. Casso, and D. Beach. 1994. KAP: a dual specificity phosphatase that interacts with cyclin-dependent kinases. *Proc. Natl. Acad. Sci. USA*. 91:1731–1735. http://dx.doi.org/10.1073/pnas.91.5.1731

Rush, J., A. Moritz, K.A. Lee, A. Guo, V.L. Goss, E.J. Spek, H. Zhang, X.M. Zha, R.D. Polakiewicz, and M.J. Comb. 2005. Immunoaffinity profiling of tyrosine phosphorylation in cancer cells. *Nat. Biotechnol.* 23:94–101. http://dx.doi.org/10.1038/nbt1046

Table S3 lists proteins differentially phosphorylated upon CDKN3 knockdown, and is available as an Excel file.